FEB 2 2005

REPORT DOCUMENTATION PAGE		Form Approved OMB No. 0704-0188

Public reporting burden for this collection of information is estimated to average 1 hour per response, including the time for reviewing instructions, searching existing data sources, gathering and maintaining the data needed, and completing and reviewing the collection of information. Send comments regarding this burden estimate or any other aspect of this collection of information, including suggestions for reducing this burden, to Washington Headquarters Services, Directorate for Information Operations and Reports, 1215 Jefferson Davis Highway, Suite 1204, Arlington, VA 22202-4302, and to the Office of Management and Budget, Paperwork Reduction Project (0704-0188), Washington, DC 20503.

1. AGENCY USE ONLY *(Leave blank)*	2. REPORT DATE 31.Jan.05	3. REPORT TYPE AND DATES COVERED MAJOR REPORT	
4. TITLE AND SUBTITLE NEURAL NETWORK CONTROL OF A PARALLEL HYBRID-ELECTRIC PROPULSION SYSTEM FOR A SMALL UNMANNED AERIAL VEHICLE		**5. FUNDING NUMBERS**	
6. AUTHOR(S) MAJ HARMON FREDERICK G			
7. PERFORMING ORGANIZATION NAME(S) AND ADDRESS(ES) UNIVERSITY OF CALIFORNIA AT DAVIS		**8. PERFORMING ORGANIZATION REPORT NUMBER** CI04-949	
9. SPONSORING/MONITORING AGENCY NAME(S) AND ADDRESS(ES) THE DEPARTMENT OF THE AIR FORCE AFIT/CIA, BLDG 125 2950 P STREET WPAFB OH 45433		**10. SPONSORING/MONITORING AGENCY REPORT NUMBER**	
11. SUPPLEMENTARY NOTES			
12a. DISTRIBUTION AVAILABILITY STATEMENT Unlimited distribution In Accordance With AFI 35-205/AFIT Sup DISTRIBUTION STATEMENT A Approved for Public Release Distribution Unlimited		**12b. DISTRIBUTION CODE**	

13. ABSTRACT *(Maximum 200 words)*

20050207 024

14. SUBJECT TERMS			**15. NUMBER OF PAGES** 24
			16. PRICE CODE
17. SECURITY CLASSIFICATION OF REPORT	**18. SECURITY CLASSIFICATION OF THIS PAGE**	**19. SECURITY CLASSIFICATION OF ABSTRACT**	**20. LIMITATION OF ABSTRACT**

The views expressed in this article are those of the author and do not reflect the official policy or position of the United States Air Force, Department of Defense, or the U.S. Government

Neural Network Control of a Parallel Hybrid-Electric Propulsion System for a Small Unmanned Aerial Vehicle

Frederick G. Harmon,[*] Andrew A. Frank,[†] Jean-Jacques Chattot,[‡] and Sanjay S. Joshi[§]
University of California-Davis, Davis, CA 95616-5294

Parallel hybrid-electric propulsion systems would be beneficial for small unmanned aerial vehicles (UAVs) used for military, homeland security, and disaster monitoring missions involving intelligence, surveillance, or reconnaissance (ISR). The benefits include increased time-on-station and range than electric-powered UAVs and stealth modes not available with gasoline-powered UAVs. A conceptual design of a small UAV with a parallel hybrid-electric propulsion system, an optimization routine for the energy use, the application of a neural network to approximate the optimization results, and simulation results are provided. The two-point conceptual design includes an internal combustion engine sized for cruise and an electric motor and lithium-ion battery pack sized for endurance speed. The flexible optimization routine allows relative importance to be assigned between the use of gasoline, electricity, and recharging. The Cerebellar Model Arithmetic Computer (CMAC) neural network approximates the optimization results and is applied to the control of the parallel hybrid-electric propulsion system. The CMAC controller saves on the required memory compared to a large look-up table by two orders of magnitude. The energy use for the hybrid-electric UAV with the CMAC controller during a one-hour and a three-hour ISR mission is 58% and 27% less, respectively, than for a gasoline-powered UAV.

Nomenclature

AR	=	aspect ratio
b	=	total number of basis functions in the association layers in the CMAC neural network
C_D	=	total drag coefficient
$C_{D,o}$	=	zero-lift drag coefficient
C_L	=	lift coefficient
$C_{L,max}$	=	maximum lift coefficient
e	=	Oswald efficiency factor
E	=	instantaneous estimate of the mean square output error of the CMAC neural network
J	=	objective function to be minimized
L	=	generalization factor, number of association layers in the CMAC neural network
n	=	number of input dimensions for the CMAC neural network
N	=	total number of possible inputs for the CMAC neural network, number of entries in a look-up table
P_{EM}	=	electric power consumption for the electric motor, W
$P_{EM\_recharge}$	=	power consumption equivalent for the engine to operate the electric motor as a generator to recharge the battery pack, W
P_{ICE}	=	power consumption equivalent for the internal combustion engine, W
PR	=	power required, W
S	=	wing area, m^2
TR	=	thrust required, N
V_{Cruise}	=	cruise speed, m/s or kts

[*] Graduate Student, Department of Mechanical and Aeronautical Engineering, One Shields Ave., Davis, CA 95616-5294.
[†] Professor, Department of Mechanical and Aeronautical Engineering, Member Grade AIAA??.
[‡] Professor and Vice Chairman, Department of Mechanical and Aeronautical Engineering, Member Grade AIAA??.
[§] Professor, Department of Mechanical and Aeronautical Engineering, Senior Member AIAA.

$V_{Endurance}$	=	endurance speed, m/s or kts
V_{Stall}	=	stall speed, m/s or kts
v_i	=	number of intervals for an input dimension of the CMAC neural network
w_j	=	activated weight in the CMAC neural network
W	=	weight of UAV, N or lbs
W_{Empty}	=	empty weight, N or lbs
W_{Fuel}	=	fuel weight, N or lbs
W_o	=	gross take-off weight, N or lbs
$W_{Payload}$	=	payload weight, N or lbs
$W_{Propulsion}$	=	propulsion system weight, N or lbs
y_{CMAC}	=	output of the CMAC neural network
$y_{Desired}$	=	desired output from the CMAC neural network
α	=	weighting factor for electricity use
β	=	weighting factor for recharging the battery pack
δ	=	training rate for the CMAC neural network training algorithm
η_{Prop}	=	propeller efficiency
ρ	=	air density, kg/m^3

I. Introduction

A hybrid-electric vehicle (HEV) is "a vehicle in which propulsion energy is available from two or more kinds or types of energy stores, sources, or converters, and at least one of them can deliver electrical energy."[1] Within the automotive industry, HEV technology is leading to vehicles with increased fuel economy and reduced emissions. The same technology would have similar benefits if applied to unmanned aerial vehicles (UAVs) used for military, homeland security, and disaster monitoring missions. The potential benefits due to the hybrid and electric-only modes include increased time-on-station, longer range, and stealth modes. A parallel hybrid-electric propulsion system for a small UAV provides increased time-on-station and longer range as compared to an electric-powered UAV such as the current Dragon Eye or Desert Hawk.[2] The internal combustion engine (ICE) is down-sized for steady-state conditions and operated near a constant torque output. The electric motor (EM) provides additional power for acceleration or climbing and serves as a generator during charge-sustaining operation or regeneration. Electric-only operation provides stealth operation not available with gasoline-powered UAVs by reducing the acoustic, smoke, and thermal signatures.[3] Also, electric-only operation eliminates exhaust emissions that could interfere with chemical-detecting sensors. The battery pack/generator that usually provides power for the avionics, flight control system, and payload now also provides propulsion energy during certain flight phases. Due to these advantages, a small UAV with a parallel hybrid-electric propulsion system enhances specific types of missions.

The current military missions for small or tactical UAVs include force protection, surveillance, and reconnaissance. The electric-powered Desert Hawk was designed for the Air Force security forces to conduct area surveillance, monitor runway approach and departure ends, and patrol base perimeters to increase the security of overseas bases.[2] Another small electric-powered UAV, the Dragon Eye, was designed to conduct reconnaissance for the Marine Corps.[2] The tactical Pioneer UAV has been used by the Navy, Army, and Marine Corps for reconnaissance and surveillance. Wilson comments that "The Navy's Pioneer, a direct derivative of Israeli surveillance and reconnaissance UAVs, played a crucial role as a spotter for U.S. battleships. They were so effective that Iraqi troops began to associate the sound of the little aircraft's two-cycle engine with an imminent devastating bombardment."[4] Additional military missions for the small or tactical UAV include intelligence, communications relay, chemical weapons detection, target acquisition, and battle-damage assessment.

A UAV with a parallel hybrid-electric propulsion system could also be advantageous for homeland security missions such as pipeline inspection, seaport surveillance, and large facility security.[4] Electric-only operation would prevent the intruders from detecting the approaching UAV and would minimize public noise disturbances when the UAV is flying over populated areas. The electric-only operation would also not interfere with highly-sensitive chemical or biological weapon sensors.

Another proposed application for the small UAV with a parallel hybrid-electric propulsion system is disaster monitoring such as the observation of forest fires. Due to the cost of the surveillance sensors, the electric system would provide redundancy for the gasoline engine when the UAV is operating in dense smoke conditions. The hybrid-electric system could potentially reduce the risk of losing expensive payloads or the UAV airframe when operating in hazardous conditions. Various agencies have begun to realize these benefits and are considering hybrid-electric projects for UAV applications.

The Defense Advanced Research Projects Agency (DARPA), the NASA Glenn Research Center, and other agencies are considering hybrid-electric propulsion systems for UAVs. DARPA's Micro Air Vehicle (MAV) project is designed to give the Army or Special Operations Forces a UAV with a reconnaissance and surveillance capability. The MAV is a vertical take-off and landing vehicle utilizing ducted fan technology. A series hybrid-electric propulsion system that includes a diesel engine, generator, electric motor, and batteries has been considered for the MAV. DARPA proposed that the electric-only operation could provide a "perch and stare" capability. DARPA also gave a contract to Boeing to consider a fuel cell-based hybrid-electric propulsion system for a UAV. This Ultra Leap project was proposed to have military as well as civilian applications. An example of a civilian application is Helios, NASA's high-altitude, long-endurance UAV built by AeroVironment, designed for telecommunications and atmospheric monitoring. These projects illustrate that various organizations are evaluating hybrid-electric propulsion for aerospace applications.

The design of the parallel hybrid-electric propulsion system and the associated controller for a small UAV has several objectives: 1) increase the range (i.e. fuel economy) 2) provide adequate time for the UAV to operate in stealth (electric-only) mode during the intelligence, surveillance, or reconnaissance (ISR) mission segment and 3) provide adequate battery power for the UAV's payload (in the air or on the ground). These objectives are directly related to two operational metrics listed in the Office of the Secretary of Defense's UAV roadmap. The parallel hybrid-electric propulsion system, depending on the mission, could meet the capability metrics of a "30% increase in time-on-station requirement with the same fuel load" and "a UAV inaudible from a 500-1000 ft slant range."[2] The first metric can be met depending on the mission and the second is satisfied in electric-only (stealth) mode.

A conceptual design of a small UAV with a parallel hybrid-electric propulsion system, an optimization routine for the energy use of the propulsion system, the application of a neural network to approximate the optimization results, and simulation results are provided. The conceptual design results in a two-point design that includes an ICE sized for cruise and an EM and battery pack sized for endurance speed. The control of the hybrid-electric propulsion system is based on an instantaneous optimization routine that uses a hyper-plane generated from the nonlinear efficiency maps for the ICE, EM, and lithium-ion battery pack. The hyper-plane incorporates charge-depletion (CD) and charge-sustaining (CS) strategies in addition to ideal operating line (IOL) concepts developed by previous researchers.[5-7] The optimization routine is flexible and allows the user to assign relative importance between the use of gasoline, electricity, and recharging. The Cerebellar Model Arithmetic Computer (CMAC) associative memory neural network is applied to the control of the parallel hybrid-electric propulsion system to approximate the nonlinear hyper-plane. The CMAC neural network saves on the required memory compared to a large look-up table (LUT) by two orders of magnitude. The CMAC controller also prevents the need to compute a hyper-plane or complex logic every time step. A Simulink model was created to compare energy use results between the various configurations and controllers.

II.   Hybrid-Electric Vehicle Configurations and Operating Strategies

The mechanical configuration of a HEV can be classified into two main categories: series and parallel (see Fig. 1).[1, 8, 9] The ICE in a series configuration acts as an auxiliary power unit to drive a generator that provides power to the energy storage system or the EM. Only the EM is connected to the mechanical drive train. The ICE is not connected to the mechanical drive path which allows it to be operated in an optimum torque and speed range. However, large energy conversion losses exist between the mechanical and electrical system diminishing the overall system efficiency.[10] Also, the EM has to be sized for the maximum power required.[8] The series configuration is useful for low-speed, high-torque applications such as buses and aircraft tow tractors. In a parallel configuration, each energy source or converter can provide propulsion energy since the ICE and EM are both mechanically connected to the drive train. The torque of the EM can supplement the torque of the ICE or additional ICE torque can operate the EM as a generator to recharge the battery pack. Because of the mechanical coupling, energy converters such as gas turbines with a relatively large turn on/off time cannot be used in a parallel configuration.[11] The speed of the drive train is not always the optimum speed for the engine, but the energy conversion losses are minimized. The ICE and EM can be sized smaller than in a series configuration and the EM is used as the generator so a separate generator is not required. The parallel configuration is used in most FutureTruck competition vehicles [12-14] and in the Honda Insight and Civic. The parallel and series hybrid configurations are the traditional configurations but others have been used such as the series-parallel configuration used in the Toyota Prius and the Nissan Tino.[15] The different configurations each have their advantages and disadvantages, and the configuration is dictated by the application and the type of energy source or converter.

An estimate was completed between a parallel and series configuration for a small UAV (≤50 lbs). The parallel configuration is lighter by ≈2.5 lbs, or 8%, of the proposed UAV's gross weight of 30 lbs. The extra weight for the

series configuration is primarily due to the required generator and the larger EM. The series configuration and controller are mechanically and electronically simpler, but the disadvantages are the weight penalty and the energy conversion losses. Harmats also concluded that the parallel configuration was more effective than the series configuration for a hybrid-electric propulsion system (solar power/EM/ICE) for a UAV.[16] The parallel configuration contains a more complicated controller and clutch/gearing mechanism but weighs less which is a significant consideration for the UAV design. The parallel configuration also does not have the significant energy losses associated with the generator and battery charging/discharging. During flight, the parallel hybrid-electric propulsion system allows the vehicle to be propelled directly with the ICE or the EM. The parallel configuration is used for the hybrid-electric UAV due to the advantages of a parallel configuration for analogous applications, the weight savings, and because of the parallel HEV experience at the University of California-Davis.
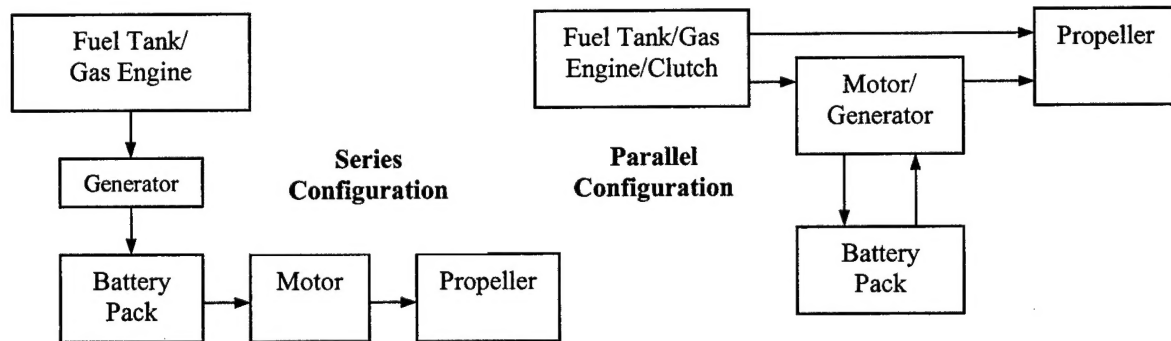
Fig. 1 Series and parallel hybrid-electric configurations

In addition to the two primary HEV configurations, three overarching operating strategies are used for the energy management of a HEV: electric-only, charge-sustaining (CS), and charge-depleting (CD).[17] The electric-only strategy depends on the ICE turn-on speed, the size of the battery pack, and the amount of low-speed operation. The electric-only strategy is available if the system is mechanically designed to permit it. The other two strategies are the hybrid approaches. The CS hybrid strategy often uses a "thermostat" approach with an attempt to maintain the battery state-of-charge (SOC) at a certain level. This approach is often used for series hybrid-electric configurations but is also used for parallel HEVs. The thermostat method allows the vehicle to be similar to conventional vehicles. If the engine is used to keep the battery at a specified SOC, the battery pack does not require charging from an external source and the operator only needs to "fill up the gas tank." In contrast to the CS strategy, the CD strategy allows the battery SOC to decrease maximizing the energy use from off-board charging. This requires the operator to plug the vehicle into an external outlet to charge the batteries, hence the name "plug-in" HEV. The CD strategy can be used in series or parallel HEVs.

The hybrid-electric UAV uses a mix of the operating strategies depending on the mission and the intent of the operator. Due to the weight limitations, a relatively large battery pack cannot be used so a purely CD strategy cannot be used. A purely CS strategy will limit the time-on-station and stealth mode duration. Sufficient SOC is required for the enemy area or whenever the stealth (electric-only) mode is required. Because of this rationale, a combination of the charging strategies is used.

III. Conceptual Design of a Parallel Hybrid-Electric Propulsion System
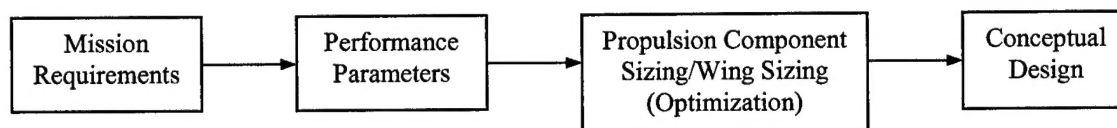
Many HEVs are conversions from stock vehicles where the original power train is removed and the appropriate components for the hybrid-electric power train are installed. Although the design for the hybrid-electric unmanned aerial vehicle (HEUAV) could take the same approach by using a large scale model aircraft or a manufacturer's UAV, this section steps through a conceptual design process for sizing the wing and the propulsion system components. The background provides a fundamental understanding of the requirements and trade-offs for the hybrid-electric propulsion system to enable a better control system design. The information in this section was presented at the Unmanned Systems North America 2004 Symposium but is included here for completeness.[18]

The conceptual design approach for aircraft is well described in Anderson, Raymer, Stinton, and Corke.[19-22] Several software packages exist such as ACSYNT[23] and RDS[24] for aircraft sizing and design. Key design variables such as wing lift coefficient, wing loading, power-to-weight ratio, and aspect ratio are optimized in the conceptual

design process. The literature reveals that defense contractors and universities have devoted much effort to the subject of conceptual design.

Conceptual design is a multidisciplinary endeavor but the focus here is the initial sizing of the wing and the hybrid-electric propulsion system components. A MATLAB routine was written to optimize the size of the wing and the propulsion system components for a conventional high-wing UAV. The HEUAV sizing problem is a constrained optimization formulation. The MATLAB optimization routine uses a sequential quadratic programming method. A quasi-Newton updating method is used at each iteration. The solution of a quadratic programming subproblem is then computed and used in a line search procedure.

```
┌──────────────┐    ┌──────────────┐    ┌──────────────────────┐    ┌──────────────┐
│   Mission    │───▶│ Performance  │───▶│ Propulsion Component │───▶│  Conceptual  │
│ Requirements │    │  Parameters  │    │  Sizing/Wing Sizing  │    │    Design    │
│              │    │              │    │     (Optimization)   │    │              │
└──────────────┘    └──────────────┘    └──────────────────────┘    └──────────────┘
```

Fig. 2 Hybrid-electric propulsion system sizing flowchart

The basic sizing of the wing and the propulsion system components for the HEUAV can be determined using a flowchart as shown in Fig. 2. To begin, the primary mission requirements of the UAV must be determined. Once the mission requirements are specified, performance parameters required to satisfy the mission can then be established. The size of the wing and the propulsion system components can be estimated based on the performance parameters. The result is a conceptual design that would undergo iterations before a detailed design is obtained.

A typical mission for a small UAV is the intelligence, surveillance, and reconnaissance (ISR) mission. A typical flight profile would be to take-off, climb to several thousand feet, cruise for an hour to the location of interest, fly at endurance speed in stealth (electric-only) mode while on station for an hour conducting ISR, and then return to base and land. The HEUAV is sized for this mission. A descent and climb could also be added before and after the ISR segment to get a closer look at the area of interest. The typical mission will be used to illustrate the concepts but the sizing process could be easily adapted to other missions.

A. Performance Requirements for the Hybrid-Electric UAV

Performance requirements to satisfy the ISR mission are used to size the wing and the propulsion system components. The size of the fuel tank, ICE, battery pack, and EM are based on the performance requirements. Table 1 includes a proposed list of the performance requirements. The hybrid-electric system components are based on the following regimes of operation:[9, 25] 1) take-off power provided by the ICE or the ICE and EM 2) climbing power provided by the ICE or the ICE and EM 3) maximum speed power provided by the ICE and EM 4) cruise power provided by the ICE-a margin is needed to recharge the batteries during CS operation 5) endurance power provided by the EM for stealth operation and 6) missed approaches and emergency power provided by the ICE and EM. The energy density and the mass of the battery pack determine the duration of the stealth mode. The ICE is sized for cruise and the EM is sized for the endurance speed. The maximum power from the motor may be needed intermittently during take-off, acceleration, maximum speed, and emergencies. These requirements were analyzed in the typical ISR mission.

Table 1   Performance parameters

Parameter	Value
Cruise Speed, kts	45-55 (23.2-28.3 m/s)
Endurance Speed, kts	20-25 (10.3-12.9 m/s)
Maximum Speed, kts	60-65 (30.9-33.4 m/s)
Rate-of-Climb, ft/min	400 (2.0 m/s)
Time for Cruise (Range), hr	1.0
Time at Endurance Speed, hr	1.0
Take-off Distance, ft	80-100 (≈24.4-30.5 m)
Payload Power, W	75
Payload Mass, lbs	3-6 (≈1.4-2.7 kg)

Weight Fractions

The weight of the UAV can be expressed using weight fractions as:[20]

$$W_o = \frac{W_{Payload}}{1 - \dfrac{W_{Fuel}}{W_o} - \dfrac{W_{Empty}}{W_o}} \tag{1}$$

Since the empty weight includes the propulsion system, Eq. (1) can be modified to separate the propulsion system weight:

$$W_o = \frac{W_{Payload}}{1 - \dfrac{W_{Fuel}}{W_o} - \left(\dfrac{W_{Empty} - W_{Propulsion}}{W_o}\right) - \dfrac{W_{Propulsion}}{W_o}} \tag{2}$$

The term, $(W_{Empty}-W_{Propulsion})/W_o$, is the glider weight fraction. Equation (2) is used to compare the weight of the original configuration (ICE only) to the hybrid-electric configuration. The propulsion system weight fraction for the original configuration includes a larger ICE, generator, and the propeller. For the parallel hybrid-electric configuration, the propulsion system weight fraction includes the down-sized ICE, clutch, batteries, EM, and the propeller. The fuel weight fraction, W_{Fuel}/W_o, is determined by computing the amount of fuel needed for each mission segment using estimates and the well known Breguet equation.[19] For the HEUAV, no fuel is used during the endurance mission segment since only electric power is required. The amount of fuel required for the mission is then used to size the fuel tank for the original and HEUAV configurations.

B. Wing and Propulsion System Component Sizing

The sizing of the wing and the propulsion system components are determined from the performance parameters. Due to the potentially large number of variables involved, several were chosen as the key parameters for the sizing process such as the wing loading, aspect ratio, maximum lift coefficient, stall speed, and endurance speed. Several constraints apply to the optimization formulation and will be discussed. The power required at the endurance speed is chosen as the objective function to be minimized. By minimizing the power required at the endurance speed, the weight fraction for the batteries will be minimized permitting a feasible payload weight. The logic and concepts involved reveal the trade-offs that must be considered to select the correct size of components for the parallel hybrid-electric propulsion system.

Since the focus of the mission is the ISR segment, the EM size and battery weight are first determined to satisfy the one hour of endurance while on station in stealth mode. The power required at the endurance speed is the objective function for the constrained optimization problem. The power required to fly at the endurance speed is given by:[19]

$$PR = \eta_{Prop} \cdot P_{EM} = \sqrt{\frac{2 \cdot W^3 \cdot C_D^2}{\rho \cdot S \cdot C_L^3}} = W \cdot \sqrt{\frac{2 \cdot W \cdot C_D^2}{\rho \cdot S \cdot C_L^3}} = W \cdot \sqrt{\frac{2}{\rho} \cdot \left(\frac{W}{S}\right)} \cdot \frac{4 \cdot C_{D,o}}{\left(3 \cdot C_{D,o} \cdot \pi \cdot e \cdot AR\right)^{0.75}} \tag{3}$$

The power required is minimized with a small wing loading, W/S, and a large aspect ratio if initial estimates for W, $C_{D,o}$ and e are available. To minimize the power, the result can be thought of as an aircraft that has a large wing area and aspect ratio such as a glider. This type of aircraft would be the most beneficial for sizing the electric system but limits other performance parameters such as the maximum speed. A compromise must be made between this geometry and a smaller wing and aspect ratio. In order to determine the power required from the batteries, it is noted that the power given by Eq. (3) does not include the propeller efficiency, motor efficiency, and the power required for the payload, avionics, and flight control system.

The parameter $C_L^{3/2}/C_D$ in Eq. (3) is referred to as the endurance parameter and is found in the literature as the key parameter for solar aircraft or any aircraft with a mission requiring it to fly near or at the endurance speed.[26] Since the ISR mission requires the HEUAV to fly near the endurance speed, the endurance parameter is critical.

Several constraints are required to complete the constrained optimization problem. The aspect ratio expressed in terms of the wing loading and the endurance speed gives the first constraint:[19]

$$\sqrt{AR} = \left(\frac{2}{\rho} \cdot \left(\frac{W}{S} \right) \cdot \sqrt{\frac{1}{3 \cdot C_{D,o} \cdot \pi \cdot e}} \right) \cdot \frac{1}{V_{Endurance}^2} \tag{4}$$

The second constraint involves the wing loading, stall speed, and the maximum lift coefficient:[19]

$$\frac{W}{S} = \frac{\rho \cdot V_{Stall}^2 \cdot C_{L,max}}{2} \tag{5}$$

The stall speed, for this application and low-speed aircraft, determines the desired wing loading.[19] The landing distance, considered not to be critical for this application, can also determine the wing loading. A safety speed margin of $\approx$3-5 kts is desired between the stall and endurance speeds to account for wind gusts and other disturbances.

The third constraint determines the size of the gasoline ICE. A margin of $\approx$125% provides extra power from the ICE to operate the EM as a generator to recharge the batteries and to provide power for the payload, avionics, and flight control system. The expression for the power required during cruise can be expressed as:

$$PR = P_{ICE} \cdot \eta_{Prop} \cdot 0.8 = V_{cruise} \cdot \left(0.5 \cdot \rho \cdot V_{cruise}^2 \cdot S \cdot C_{D,o} + \frac{S}{0.5 \cdot \rho \cdot V_{cruise}^2 \cdot \pi \cdot e \cdot AR} \cdot \left(\frac{W}{S} \right)^2 \right) \tag{6}$$

where PR=$V_{cruise} \cdot$TR at cruise speed. Using S=S·W/W, Eq. (6) becomes:

$$PR = P_{ICE} \cdot \eta_{Prop} \cdot 0.8 = 0.5 \cdot \rho \cdot V_{cruise}^3 \cdot W \cdot C_{D,o} \cdot \frac{S}{W} + \frac{W}{0.5 \cdot \rho \cdot V_{cruise} \cdot \pi \cdot e \cdot AR} \cdot \left(\frac{W}{S} \right) \tag{7}$$

For maximum speed, the EM and ICE are both used. The EM can tolerate an over-torque for short durations so the expression for the maximum speed is the same as Eq. (7) except PR=$P_{ICE} \cdot \eta_{Prop}$+over_torque·$\eta_{Prop} \cdot P_{EM}$. Typical values for the over-torque factor are 1.5-2.0.

The objective function and the third constraint form the foundation for a two-point design for the HEUAV. The EM and battery pack of the propulsion system are sized based on the endurance speed and the ICE is sized based on the cruise power requirements. The optimization routine determines the optimum design between the two design points.

C. Optimization and Conceptual Design Results
The conceptual design results based on the constrained optimization problem led to the results shown in Table 2 for an altitude of 5 kft MSL. Limits were placed on the optimized variables and the results show that the optimization routine used the lowest wing loading available. The size of the wing is directly related to the wing loading. A large wing is desired but other performance parameters must be considered along with the structural, weight, and low observable requirements. Limits were placed on the maximum lift coefficient in an attempt to obtain results that would permit a standard NACA, Eppler, or Selig airfoil to be used.[27, 28] Other high lift wings could be used such as the low Reynolds number NASA LRN-1-1010 airfoil used in the Navy's low altitude unmanned research aircraft (LAURA) project.[29] The optimization results either meet or exceed the performance requirements listed in Table 1. The endurance speed from the optimization routine is less than the stall speed which is physically not realistic but was permitted to obtain realistic values for the power required at endurance speed. The power required to fly 3-5 kts above the stall speed instead of precisely at the endurance speed is minimal. The power requirements for each mission phase are shown and are used to size the different components. A smaller ICE and less fuel can be used for the HEUAV as compared to the original configuration. The HEUAV requires 25% less fuel than the original configuration for the same mission but with a reduced payload.

The hybrid-electric propulsion system is a two-point design with the electric system sized for endurance speed and the ICE sized for cruise speed. The two design points are shown in Fig. 3. The endurance speed of ≈25 kts (12.9 m/s) occurs near the minimum power required of 85 W (see Fig. 3). The EM and battery pack are sized for this speed with additional power for the avionics, payload, and flight control system. The gasoline ICE is sized for a cruise speed of 50 kts (25.7 m/s) which requires ≈500 W not including the inefficiencies of the propulsion system and the margin required for CS operation.

Table 2   30 lb HEUAV optimization and conceptual design results

Parameter	Value
Optimization Routine Results	
Aspect Ratio	14.6
Wing Loading, N/m^2	90 (30 oz/ft^2)
Max Lift Coefficient, $C_{L,max}$ (finite wing)	1.25
Oswald Efficiency Factor	0.85
Zero-lift Drag Coefficient	0.036
Stall Speed, m/s	11.7 (22.7 kts)
Endurance Speed, m/s	9.1 (17.7 kts)
EM Power at Endurance Speed, W	114
ICE Power Estimate at Cruise Speed, W	837
Conceptual Design Results	
Wing Area, m^2	1.48 (15.9 ft^2)
Wing Span, m	4.65 (15.3 ft)
Wing Chord, m	0.32 (12.5 in)
Endurance Parameter	20.4
Max L/D Ratio	16.4
PR for Take-Off[a], W	503
PR for Climb[a], W	356
PR for Cruise[a], W	502
PR for Endurance[a], W	85
PR for Max Speed[a], W	852
Nominal Propeller Efficiency, %	75
Original Fuel Mass, kg	2.0 (71 oz)
HEUAV Fuel Mass, kg	1.5 (53 oz)
Original Payload Mass, kg	3.0 (6.6 lbs)
HEUAV Payload Mass, kg	1.9 (4.2 lbs)
Original ICE Power Required, W	1230 (1.7 hp)
HEUAV Battery Mass[b] kg	2.2 (4.9 lbs)
HEUAV Battery Storage[b], Wh	220

[a]The PR does not include propulsion system inefficiencies or the PR for the avionics and payload.
[b]The battery storage requirement includes the power needed for the avionics and payload.

The weight fractions required for the original configuration and the HEUAV configuration are shown in Fig. 4. The glider weight fraction is statistically estimated from several long endurance UAVs in the same weight class with an empty weight of 0.63. The propulsion weight fraction for the original configuration is 0.12 less than the HEUAV configuration. The fuel weight fraction is 0.11 for the HEUAV and 0.15 for the original (ICE only) configuration. For comparison, the fuel weight fraction can be as large as 0.35 for long-endurance UAVs. The advantages of the HEUAV configuration must be weighed against the loss in payload mass for a particular mission. The weight fractions for the HEUAV propulsion system components are shown in Fig. 5. Less fuel is required for the HEUAV but the battery weight is significant with a weight fraction of 0.16.

Commercial off-the-shelf components are matched to the optimization simulation results and are shown in Table 3. Nominal design values based on the results from the optimization routine and the components in Table 3 are used for the HEUAV propulsion system simulations. The ICE, EM, and battery pack are slightly larger than required but will ensure the power requirements are met for the intended mission.
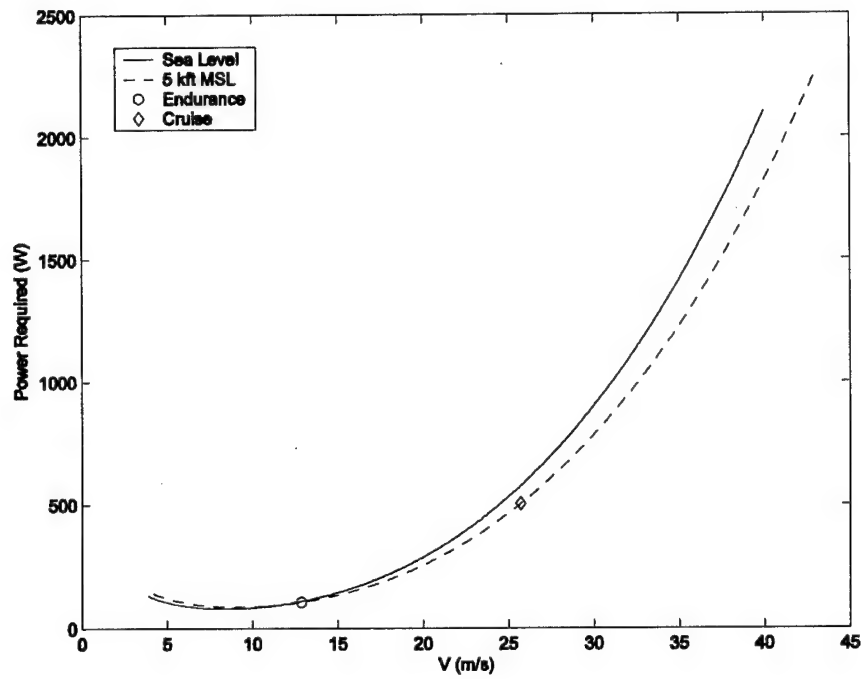
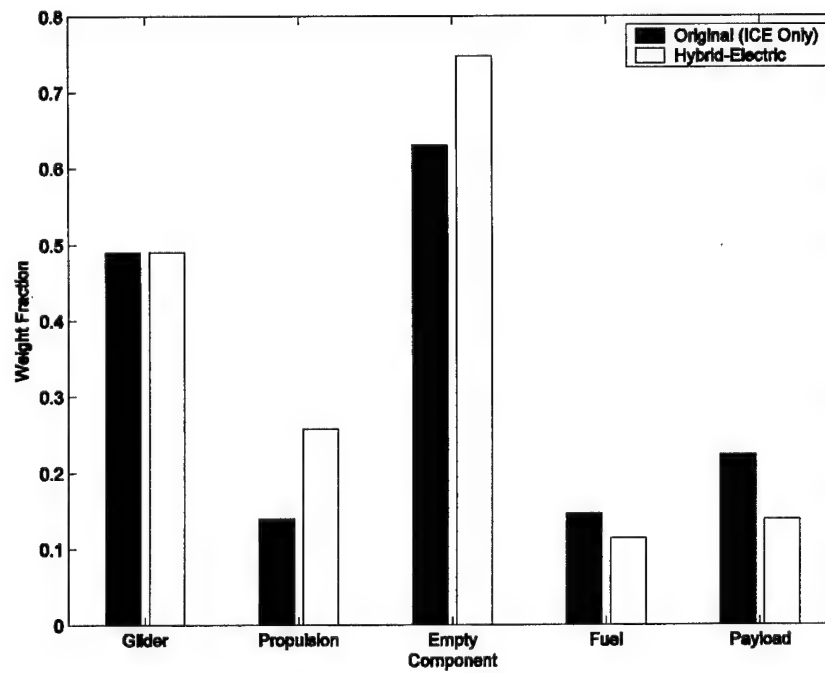**Fig. 3 Power required at sea level and 5 kft MSL for the hybrid-electric UAV**

Fig. 4 Weight fraction comparison, normalized to UAV weight (W_o=30 lbs)
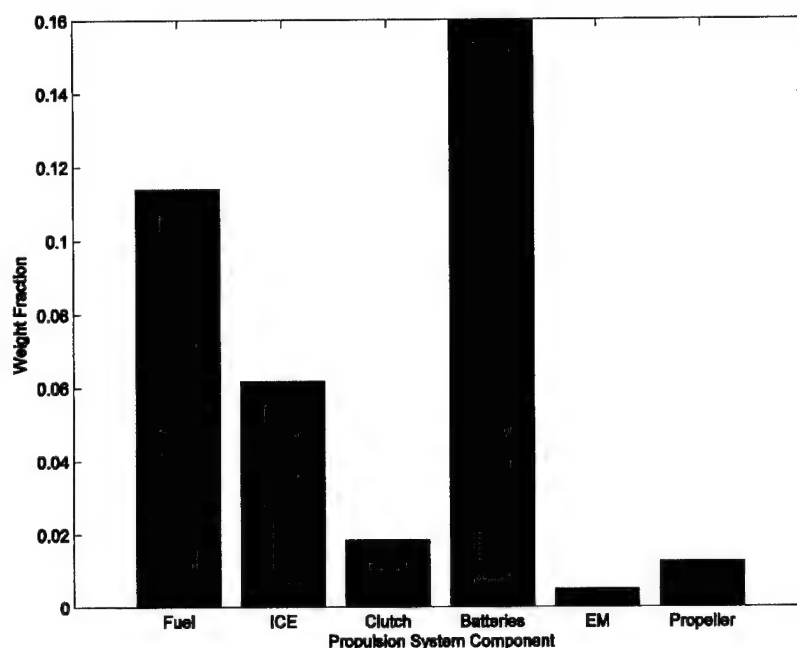
Fig. 5 Weight fractions for the HEUAV propulsion system (W_o=30 lbs)

Table 3   Commercial off-the-shelf components for 30 lb HEUAV

Parameter	Value	Parameter	Value
Airframe	Conventional High-Wing Aircraft	**Battery Pack**	Ultralife UBI-2590 (2 in Parallel)
Mass, kg	13.6 (30 lbs)	Type	Li-Ion, Rechargeable
Oswald Efficiency Factor	0.85	Mass, kg	1.44·2=2.88 (6.3 lbs)
Zero-lift Drag Coefficient	0.036	Voltage, nominal, V	14.4
Wing/Airfoil	NACA 23012, E214, S2091, or SD7032	Voltage Range, V	12.0 to 16.4
$C_{L,max}$	1.25 (3-D, Re=150k)	Capacity, C/2.5, Ah	10·2=20
Aspect Ratio	14.6	Energy Density, Wh/kg	100
Wing Area, m^2	1.48 (15.9 ft^2)	Recommended Discharge Current, A	8·2=16 A
Wing Span, m	4.65 (15.3 ft)	**Electric Motor (3.7:1 Gearbox)**	Aveox 2739/3Y Brushless DC
Wing Chord, m	0.32 (12.5 in)	Mass, kg	0.16 (5.6 oz)
Payload		Max Peak Current, A	30
Original Payload Mass, kg	2.9 (6.4 lbs)	Max Continuous Current, A	22
HEUAV Payload Mass, kg	1.7 (3.7 lbs)	Winding Resistance, Ω	0.0817
Original Generator/Battery Mass, kg	0.5	No Load Current, A	0.90
Avionics and Payload Power, W	75	Speed Constant, rpm/V	1134
Engine (Two-Stroke, Gasoline)	First Place Engines	Torque Constant, in-oz/A	1.19
Displacement, cm^3	21 (1.3 in^3) (Original-35)	Motor Constant, in-oz/sqrt(W)	4.28
Mass, kg	1.13 (2.5 lb)	Maximum Speed, rpm	50,000
Fuel Tank Mass, oz	54 (Original-74)	**Propeller**	Maple, 18x10
Clutch (Electromagnetic)	RM Hoffman Co.	Mass, kg	0.17 (6 oz)
Mass, kg	0.25 (0.55 lbs)	**Horizontal and Vertical Stabilizer/Airfoil**	NACA 0009

A two-stroke gasoline engine was matched to the optimization results since the fuel is available at military installations and because the engines are readily available. A four-stroke gasoline engine is used in the simulations in a following section but the more efficient engine is heavier and the payload capacity is decreased. Attempts are being made to design small heavy fuel engines for UAVs so that they use similar fuels as other military vehicles instead of gasoline. D-Star Engineering has designed and built a 0.07 kW and a larger 1 kW diesel engine intended for UAVs.[30] For the purposes of the conceptual design, typical performance of a two-stroke gasoline engine was used but the conceptual design approach could be easily adapted to other types of engines.

A conceptual approach to the sizing of the UAV wing and propulsion system components was discussed in this section. An optimization problem with constraints was formulated to minimize the power required at or near the endurance speed. The weight of the battery pack was minimized with this approach. The optimization and conceptual design results were matched to off-the-shelf components which are used in the simulations. The background explained in this section gives a more fundamental understanding of the requirements and trade-offs for the hybrid-electric propulsion system to enable a better control system design.

IV. Control Algorithms for Hybrid-Electric Propulsion Systems

The hybrid-electric vehicle operating strategies (electric-only, CS, and CD) are overarching approaches. For each operating strategy, control algorithms are used to optimize the energy or power use of the propulsion system. In addition to rule-based or logic-based strategies, several advanced control approaches have been reported in the literature for the control of HEV power trains in automotive applications: 1) optimal control 2) fuzzy logic 3) adaptive control 4) nonlinear control and 5) genetic algorithms. A brief overview of each and their application to the control of HEV power trains is given by Harmon[31].

The goal of an advanced control system is to use a minimal amount of energy by finding the best combination of motor torque and engine torque as a function of rotational speed, battery SOC, torque demand, or other parameters. Of the hybrid-electric power train advanced control schemes appearing in the current literature, those based on artificial neural networks (ANN) or fuzzy logic appear to be the most promising due to the relatively low computational resources needed and because an accurate power train propulsion model is not required (an accurate model is required for simulations). These approaches are also useful for nonlinear and multivariable systems, can learn, and generalize. Even though results from many of the other control methods such as optimal control are very good, the computational requirements are too excessive for the embedded microcontrollers and the majority of the theory is for linear models.

The use of ANNs in HEV applications has been limited and due to the potential benefits, this particular control method was selected for the HEUAV application. It is well known that ANNs can approximate nonlinear functions so an ANN has tremendous potential if applied to the control of the nonlinear HEUAV propulsion system. A specific type of neural network, the Cerebellar Model Arithmetic Computer or Cerebellar Model Articulation Controller (CMAC), was chosen for this application due to its rapid training time, practical hardware implementation, and low computational cost.[32] The CMAC is an alternative to the more common back-propagation multilayer network.[33] The CMAC ANN, described in the next section, has been successfully applied to industrial applications, vibration control, robotic control, and fuel-injection systems.[34-37]

V. Overview of the CMAC Neural Network

The CMAC is a feed-forward, supervised ANN and is an alternative to the more common back-propagation multilayer perceptron network.[33] The CMAC was originally developed to adaptively control robots since it can handle large input spaces, adapt, learn quickly, generalize, and is stable. Before the advantages of the CMAC are discussed in more detail, the disadvantages of the back-propagated multilayer perceptron ANN for a real-time application will be discussed. First, the common back-propagated ANN is usually not feasible for on-line learning since numerous iterations are needed for the ANN to converge during training. Please note that on-line learning is not used for the HEUAV application but could be an area of future research. Second, many calculations are needed per training iteration for the back-propagated ANN which can necessitate custom hardware. Third, the commonly used training algorithms for back-propagation are based on gradient techniques and the neural network can get "stuck" in a relative minimum during training vs. converging to the global minimum on the error surface. Fourth, it has been shown that the local learning approaches used in the CMAC ANN and other associative memory networks are superior for control applications as compared to those used in the multilayer ANNs.[38] Fifth, the computational time needed to produce an output from the CMAC ANN is minimal since only a few calculations are needed to obtain the output for an input. For these reasons, the CMAC was selected for the HEUAV application instead of the back-propagated multilayer ANN.

The CMAC neural network was originated by James Albus in 1975.[39, 40] The CMAC is modeled after the method that the cerebellum uses to learn and store information and control reflexive movement which is in contrast to a traditional neural network that attempts to mimic the interactions between the brain's neurons. The CMAC ANN attempts to duplicate the functional properties of the brain instead of the structure of it.[40] The CMAC ANN can be thought of as an adaptive look-up table (LUT). The CMAC is better suited to real-time control as compared to a LUT for two reasons: the CMAC can generalize whereas a LUT cannot and the CMAC requires much less memory than a LUT for large input spaces.

The CMAC is a lattice-based associative memory network that nonlinearly maps the inputs to a hidden associative memory. The hidden memory is then linearly mapped to an adaptive weight vector that generates the output. The output is the sum of the activated weights. For each input, only a small subset of the network influences the instantaneous output which minimizes the computational time which is a significant benefit for an embedded controller. Whereas the computational cost for most neural networks is exponentially dependent on the dimensions of the input space, the computational cost for a CMAC is linearly dependent on the input space dimensions.[41] In short, the CMAC takes real-valued vectors and produces real-valued output vectors, can learn locally and generalize, can learn nonlinear functions, has a relatively short training time, requires a small number of computations per training iteration, and can be implemented in simple software and hardware.[32] The number of training iterations is orders of magnitude smaller than that of other ANNs.[33, 42] The CMAC ANN is applied to the control of the HEUAV propulsion system to produce commands for the propulsion system components.

A diagram of a typical CMAC neural network is shown in Fig. 6. Continuous vectors are first transformed into quantized input vectors. The maximum and minimum values of the inputs (range) are needed along with the quantization width (precision or resolution) of the inputs to determine the size of the input space.[35] The input space is n-dimensional if more than one input is fed to the CMAC structure. Second, the input space is nonlinearly mapped into exactly L locations (generalization factor) in the associative memory satisfying the uniform projection principle. Please note that the nonlinear mapping in a CMAC structure occurs in the initial mapping and not in the sigmoid/threshold function of a neuron as in other types of ANNs. Each of the association cells (also referred to as basis functions with support or receptive fields) within each parallel layer of the memory has a corresponding weight. Each association cell has a support area of L^n where n is the dimension of the input space. Third, for each possible input, the weights corresponding to the L activated memory locations are then summed to form the output. The weights mapped to each memory location determine the output and are adaptively updated. The output is linearly dependent on the adaptive weights and therefore allows convergence conditions to be established.[41] It is emphasized that the nonlinear fixed mapping occurs from the input space to the association layer and the adaptive linear mapping occurs from the association layer and the associated weights to the output.
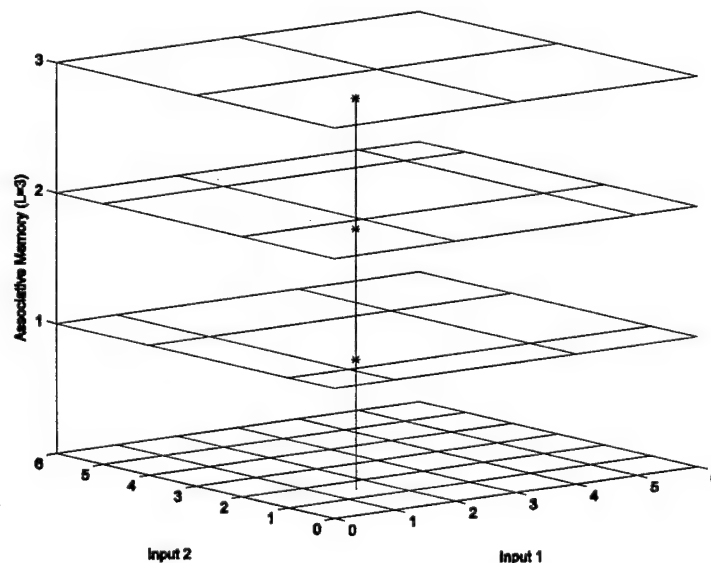

Fig. 6 CMAC neural network structure

The CMAC structure parameters typically have the following relationship for a controls application:

$$n \leq L < b < N \tag{8}$$

The example in Fig. 6 has parameters of n=2, L=3, b=22, and N=36. The total number of basis functions, b, is determined by summing the number of basis functions for each association layer. The total number of possible inputs, N, is found by multiplying the number of intervals, v_i, in each direction as follows:

$$N = \prod_{i=1}^{n} v_i \tag{9}$$

where N is the number of entries that would be found in a LUT. The CMAC is considered well defined if $1 \leq L \leq \max(v_i)$ for $1 \leq i \leq n$.[41] If the CMAC is not well defined, then a basis function will cover a relatively large area of the input space.

The distribution of the association layers is determined by a displacement vector. The original Albus scheme offset the layers by one from each other. For example, the displacement vector is (1,1,1), (2,2,2), and (3,3,3) for the example in Fig. 6. The original scheme satisfies the uniform projection principle but does not produce results as good as other schemes. Parks and Militzer produced tables of displacement vectors as a function of L and n.[43] Their displacement vectors are based on the distances between the elements in the association vectors and elements in the input space. The placement of the overlays is optimized by directly relating the Hamming distance (absolute value of the differences of each component) between the association vectors to the Euclidian distance between the input values.[33, 43] The improved displacement vectors generally produce a smoother approximation to a function.

Several techniques can be used to update the weights in the CMAC structure. For the results in this paper, the CMAC's weights are updated using an instantaneous gradient descent method to minimize the mean square error (MSE). The instantaneous estimate of the MSE is described using.[35]

$$E = \frac{1}{2} \cdot (y_{Desired} - y_{CMAC})^2 \tag{10}$$

Taking a partial derivative with respect to an activated weight, w_j:

$$\frac{\partial E}{\partial w_j} = -(y_{Desired} - y_{CMAC}) = -\left(y_{Desired} - \sum_{i=1}^{L} w_{i,Activated}\right) \tag{11}$$

Only local learning occurs since only the activated weights are updated. The resulting first-order update training rule using the instantaneous gradient descent method is:[41]

$$w_{j,updated} = w_{j,previous} + \frac{\delta}{L} \cdot (y_{Desired} - y_{CMAC}) \tag{12}$$

The learning algorithm requires minimal memory and computational cost.

The CMAC generalizes due to the width and overlap of the association cells in the hidden layers.[40] The generalization is determined by the initial nonlinear mapping since each basis function or association cell has a pre-determined corresponding support or receptive field. The supports each have a volume of L^n or less if on the edge of the input space. Therefore, the generalization parameter, L, determines the number of association layers, the number of weights contributing to each output, and the size of support for each basis function.[41] If two inputs are relatively close to each other in the input space, then approximately the same association cells will be activated to produce an output. For two inputs that are spaced far apart, entirely different association cells are activated. The CMAC generalizes over a small area which minimizes the computations required for each training iteration. However, if L is large, the generalization is less local but the memory requirement is less.

The CMAC neural network approximations will include modeling errors. The initial nonlinear mapping affects the modeling capabilities. The generalization parameter and the displacement vector also influence the modeling capabilities. As L increases, the generalization is less local and the modeling error typically increases. For a LUT, L=1, and there is no error. The flexibility of the CMAC decreases as L increases due to the decreased generalization. The advantage is the decreased memory requirement. The instantaneous gradient descent training method also introduces errors into the modeling capability. For most applications including the present HEUAV application, the modeling error is low even if the CMAC cannot model the function exactly if the appropriate parameters are chosen for the number of layers, the learning rate, and the structure of the hidden layers.

In addition to comparing performance and energy use between the rule-based and the CMAC controller, the microprocessor memory requirements are analyzed for the CMAC ANN controller. A typical processor such as the Motorola MPC555 has $\approx$512 KB of flash memory and if each CMAC weight is assumed to be a float value requiring 4 bytes (32 bits), the allowable size of the associative memory in the CMAC can be determined. The approximation $N/L^{(n-1)}$ gives the number of weights.[41] To produce an output, the weights stored in L memory locations are summed. As can be seen, the CMAC greatly saves on memory and computational requirements as compared to having a multidimensional LUT or computing a hyper-plane for every instant in time.

VI.   Optimization Algorithm and CMAC Approximations

Using the conceptual design results as a foundation, this section covers the design of the CMAC neural network controller and how it is used to approximate a control surface generated from an optimization routine. The optimization of the energy use is achieved by minimizing the instantaneous rate of energy consumption (i.e. using the total power consumption as the objective function to be minimized). The separate nonlinear efficiency maps for the ICE, EM, and battery pack are used in an off-line optimization routine to minimize the power consumption by determining the torque split between the ICE and EM during hybrid-electric operation. The optimization results are used to generate a control surface for the engine and motor torque commands. A CMAC neural network approximates the optimal control surface and is used in the simulations. Two flight profiles are used in the Simulink model to compare the CMAC neural network controller results to the rule-based controller results.

The energy available in the small HEUAV is either from the gasoline or the electrical energy stored in the battery pack. To provide power to the propeller, the energy can take one of three paths. For Path 1, energy stored within the gasoline is used by the ICE to deliver power directly to the propeller (see Fig. 7). Electrical energy can be delivered directly to the propeller via Path 2. Path 3 uses the ICE and EM to recharge the battery pack. The stored electrical energy is delivered to the propeller at a later time and for the HEUAV, the electrical energy is assumed to be delivered to the propeller at endurance speed (stealth mode).
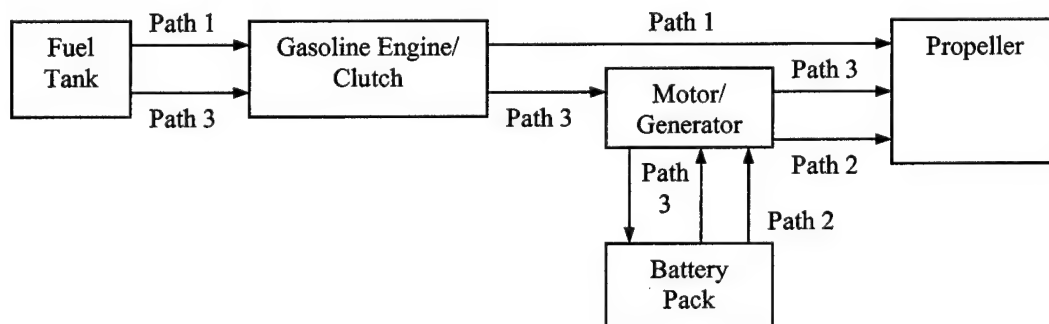

Fig. 7 Energy paths available in the parallel hybrid-electric system

The nonlinear efficiency maps for the ICE, EM, and battery pack are used in the optimization algorithm. The maps are stored in tables and interpolation is used to calculate the efficiency at specific points in the input space (i.e. demanded torque, rotational speed, and battery SOC) during the off-line optimization calculations. The ICE efficiency maps are derived from estimates and engine manufacturer dynamometer tests. Four-stroke ICE efficiency maps are used in the simulations. The efficiency map for the four-stroke engine was derived from literature for the Honda GX31, 31 cm^3 (1.9 in^3), engine. The best fuel consumption is $\approx$350 g/kWh or a maximum efficiency of $\approx$24%. The EM (Aveox 2739/3Y) efficiency map is derived from manufacturer data and has a maximum efficiency of $\approx$90%. The battery pack used in the simulations consists of two lithium-ion batteries (Ultralife UBI-2590) in

parallel. Data from the manufacturer and a battery model were used to develop an efficiency map for the battery pack. The efficiency of the battery pack decreases with either an increase in discharging or charging current.

The simple rule-based controller has two inputs: demanded torque and rotational speed. The engine is operated on a line of maximum efficiency, referred to as the Ideal Operating Line (IOL), unless the demanded torque is less than the IOL torque or if the demanded torque is greater than the combined IOL torque and maximum motor torque. Only the ICE generates torque if the demanded torque is less than the IOL torque. If the demanded torque is greater than the combined IOL torque and the maximum motor torque, then additional torque from the ICE is provided. The rule-based controller logic does not include any recharging so it is considered a CD strategy. If the mission requirements cannot be met with CD only, then a CS algorithm is used. The CS algorithm is based on the expected length of the mission and the battery SOC. A proportional-derivative (PD) controller, with the SOC as the input, is used to determine the amount of recharging required.

The CMAC controller algorithm uses the battery SOC as an input in addition to the demanded torque and rotational speed. The algorithm minimizes the total power consumption of the engine and the motor:

$$J = P_{ICE} + \alpha \cdot P_{EM} + \beta \cdot P_{EM\_recharge} \tag{13}$$

P_{ICE} is the power consumption equivalent (33.44 kWh/gallon of gasoline) of the engine to rotate the propeller (Path 1 in Fig. 7). P_{EM} is the electrical power consumption of the EM (Path 2) whereas $P_{EM\_recharge}$ is the power consumption equivalent for the engine to operate the electric motor as a generator to recharge the battery pack (Path 3). The weighting factors, α and β, penalize the amount of electricity use and the amount of recharging, respectively. If the torque of the engine is greater than the demanded torque, the motor is used as a generator to recharge the batteries.

The flowchart for the optimization routine is shown in Fig. 8. The calculations involved such as numerous table look-ups and interpolations would be excessive for an embedded microcontroller (see pg. 35 in Ref. 17). For the appropriate branches of the flowchart, the objective function is calculated in the off-line optimization by stepping the engine torque by 0.02 N·m increments to determine which torque split will minimize the power use. The values used for α and β depend on the type of mission. If the mission is a relatively short mission, values that encourage CD are used but if a longer mission is required, different values are used to produce a CS control surface. For both cases, more charging can be produced as the battery SOC decreases.

To implement the CMAC controller, various parameters are chosen such as the inputs, quantization widths, generalization parameter, and learning rate (see Table 4). The parameters chosen determine the accuracy of the CMAC approximation for the control surface function. Brown and Harris state that "that most reasonable choices give acceptable results."[41] Simulations using the original configuration (ICE only) were useful for designing the input space for the CMAC controller. By determining the range of various parameters such as the propeller speed and demanded torque, an efficient structure was developed for the CMAC neural network.

Table 4   Parameter summary for the CMAC neural network controller

Parameter	CMAC Controller
Output	Commanded Engine Torque
Inputs	Rotational Speed
	Demanded Torque
	Battery State-of-Charge
Input Ranges	Speed: 190-880 rad/s
	Torque: 0-2.5 N·m
	SOC: 2-100%
Input Resolution	Speed: 10 rad/s
	Torque: 0.05 N·m
	SOC: 2%
Number of Input Cells, N^a	70·51·50=178,500
Generalization Factor, L^b	3, 7, 9, 14, 19, 25
Learning Rate, δ	0.05
Training Iterations	150-200

[a]Entries required for a Look-Up Table (LUT)
[b]The generalization factors correspond to displacement vectors that provide a CMAC structure of good quality.

The CMAC controller inputs chosen were those that would be measurable with relatively inexpensive components. These inputs include rotational speed, demanded torque, and the battery SOC. The torque output of the ICE and EM could be useful but experience with hybrid-electric automobiles illustrate that it is reasonable to use steady-state performance maps for the propulsion system components.
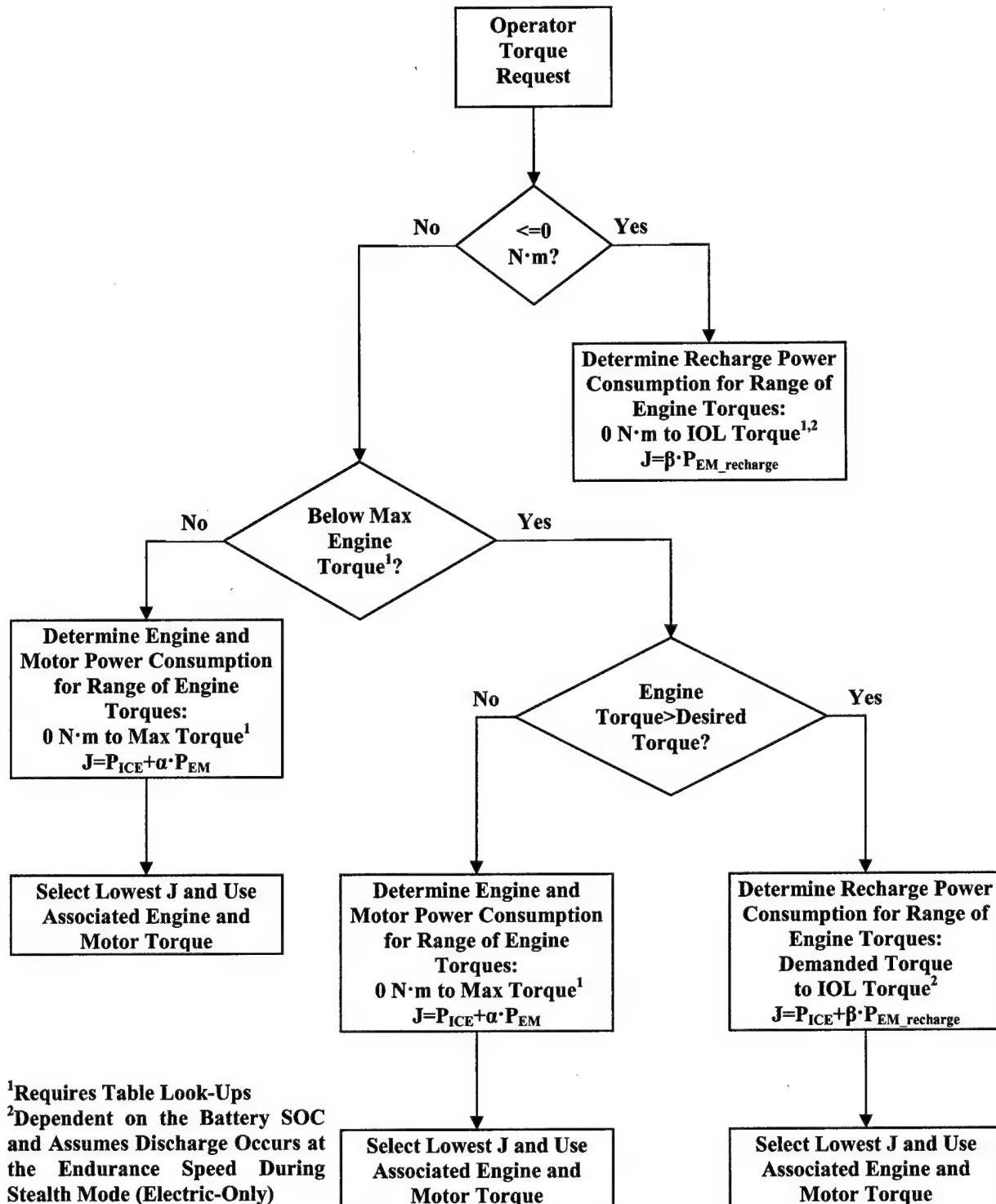
```
                        ┌──────────────┐
                        │   Operator   │
                        │    Torque    │
                        │   Request    │
                        └──────┬───────┘
                               │
                  No        ◇ <=0 ◇        Yes
              ┌──────────────  N·m?  ──────────────┐
              │                                     │
              │                        ┌────────────────────────────┐
              │                        │ Determine Recharge Power   │
              │                        │ Consumption for Range of   │
              │                        │   Engine Torques:          │
              │                        │ 0 N·m to IOL Torque^{1,2}  │
              │                        │   J=β·P_EM_recharge        │
              │                        └────────────────────────────┘
```

$J=\beta \cdot P_{EM\_recharge}$ — Determine Recharge Power Consumption for Range of Engine Torques: 0 N·m to IOL Torque[1,2]

Below Max Engine Torque[1]?

No — Determine Engine and Motor Power Consumption for Range of Engine Torques: 0 N·m to Max Torque[1] $J=P_{ICE}+\alpha \cdot P_{EM}$

Yes — Engine Torque>Desired Torque?

No — Determine Engine and Motor Power Consumption for Range of Engine Torques: 0 N·m to Max Torque[1] $J=P_{ICE}+\alpha \cdot P_{EM}$

Yes — Determine Recharge Power Consumption for Range of Engine Torques: Demanded Torque to IOL Torque[2] $J=P_{ICE}+\beta \cdot P_{EM\_recharge}$

Select Lowest J and Use Associated Engine and Motor Torque

Select Lowest J and Use Associated Engine and Motor Torque

Select Lowest J and Use Associated Engine and Motor Torque

[1]Requires Table Look-Ups
[2]Dependent on the Battery SOC and Assumes Discharge Occurs at the Endurance Speed During Stealth Mode (Electric-Only)

Fig. 8 CMAC controller optimization algorithm

Four-Stroke Engine, Charge-Depletion Approximations: CMAC approximation results for CD operation using the four-stroke engine are shown in Table 5. Weighting factors of $\alpha=3+1\cdot(1\text{-SOC})$ and $\beta=2\cdot\text{SOC}$ were determined for CD operation to permit the HEUAV to complete a shorter one-hour mission. The runs for L=3 and 7 used 200 training iterations and the other runs used 150 iterations. The CMAC approximations for L=14, 19, and 25 save on at least two orders of magnitude of memory as compared to a LUT generated from the optimization routine.

Table 5   Summary of the CMAC approximation results, four-stroke engine, charge-depletion

Generalization Parameter	RMS Error	Displacement Vector	Weights in Associative Memory	Memory Savings[a]
3	$2.50\cdot10^{-2}$	(1,1,1)	21,767	8.20
7	$4.42\cdot10^{-2}$	(1,2,3)	4,888	36.5
9	$5.25\cdot10^{-2}$	(1,2,4)	3,266	54.7
14	$6.53\cdot10^{-2}$	(1,3,5)	1,696	105.2
19	$7.69\cdot10^{-2}$	(1,3,7)	1,137	157.0
25	$8.82\cdot10^{-2}$	(1,3,8)	828	215.6

[a]Number of entries in a LUT/number of weights for the CMAC associative memory

The approximation to the original control surface gets worse as the generalization factor increases. As a cell in the associative memory covers more of the input space, the approximation gets worse as is shown by the increase in the RMS error. An example of the CD control surface for a SOC of 100% is shown in Fig. 9 for L=9. If discontinuities exist such as in the control surface for the engine, a smaller generalization factor must be used to minimize the RMS error. The CD surfaces for L=3, 7, 9, 14, and 19 produced acceptable results. A generalization factor of L=25 allowed the battery SOC to drop to a very low value and since a cell covers half of the input space for the third input dimension, L=25 is too high of a generalization factor for this application.
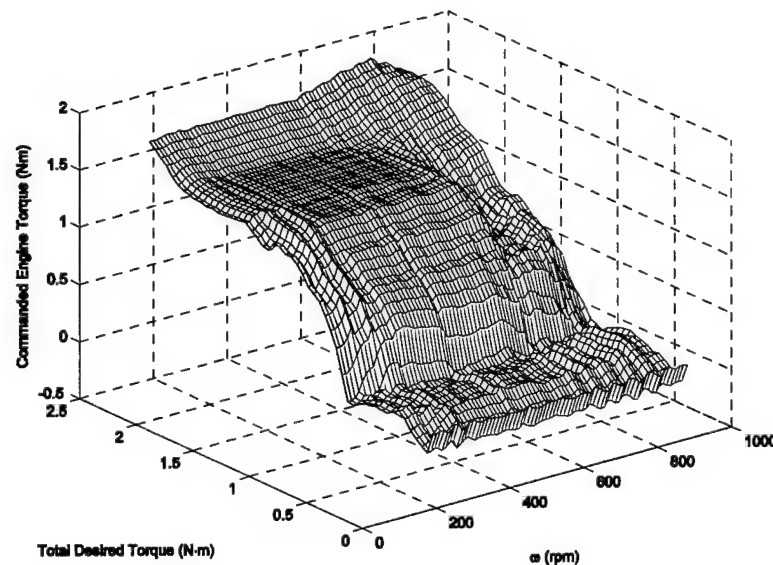
Fig. 9 CMAC approximation (L=9) for engine torque control surface, four-stroke, charge-depletion, SOC=100%

Four-Stroke Engine, Charge-Sustaining Approximations: A summary of the CMAC approximation results for the CMAC controller using the four-stroke engine are shown in Table 6. CS weighting factors of $\alpha=4+4\cdot(1\text{-SOC})$ and $\beta=0.3\cdot\text{SOC}$ permit the HEUAV to complete a three-hour ISR mission. The runs for L=3, 7, and 9 used 200 training iterations and the other two runs used 150 iterations. The CMAC approximation for L=14 and 19 saves on at least two orders of magnitude as compared to a LUT.

Table 6   Summary of the CMAC approximation results, four-stroke engine, charge-sustaining

Generalization Parameter	RMS Error	Displacement Vector	Weights in Associative Memory	Memory Savings[a]
3	$2.23 \cdot 10^{-2}$	(1,1,1)	21,767	8.20
7	$3.81 \cdot 10^{-2}$	(1,2,3)	4,888	36.5
9	$4.52 \cdot 10^{-2}$	(1,2,4)	3,266	54.7
14	$5.97 \cdot 10^{-2}$	(1,3,5)	1,696	105.2
19	$7.29 \cdot 10^{-2}$	(1,3,7)	1,137	157.0

[a]Number of entries in a LUT/number of weights for the CMAC associative memory

An example for the SOC of 25% is shown in Fig. 10 for L=14. A generalization factor of L=19 did not produce acceptable results. The surface approximation was not accurate enough to produce the desired torque commands for cruise and CS operation. The battery SOC dropped to zero since not enough recharging was generated to complete the three-hour ISR mission.
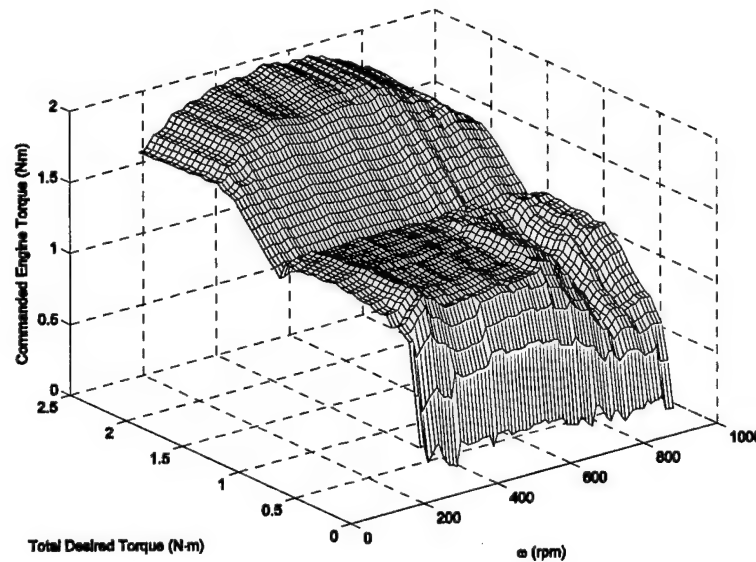
Fig. 10   CMAC approximation (L=14) for engine torque control surface, four-stroke, charge-sustaining, SOC=25%

VII.   Flight Profiles and Simulation Results

A. Flight Profiles

The small HEUAV is sized for a typical ISR mission. Two ISR missions are used to demonstrate the capabilities of the HEAUV and to compare the results of the various hybrid-electric propulsion system controllers.

The Simulink model developed for the HEUAV includes an option for the original configuration (ICE only). The ICE is sized larger than the engine used in the hybrid-electric version. The results for the HEUAV using the different controllers will be compared to the original configuration (ICE only). For the rule-based controller, logic must be programmed to determine when CS is allowed. The flexibility in the objective function for the three-input controller shows how the CMAC controller can be trained depending on the expected mission length and requirements. Separate logic for the three-input controller to enable CS is not needed since it is inherent in the optimization routine.

To show initial results for the various mission segments of a flight profile, a short one-hour ISR mission was generated (see Fig. 11). The flight profile consists of a take-off, climb, cruise, endurance speed, high speed dash, descent, and landing. The cruise speed is designed to be 50 kts and the endurance speed 25 kts. At endurance speed, the hybrid-electric UAV operates in electric-only (stealth) mode. The design altitude is 5 kft mean sea level (MSL)

and for this flight profile, the UAV takes off from 4 kft MSL. A climb and descent prior to the endurance mission segment simulate the flight over an obstacle.
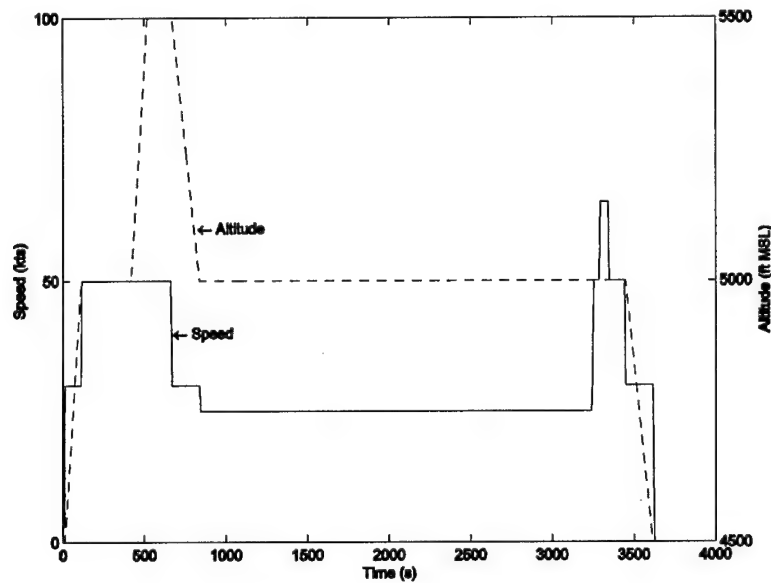
Fig. 11   One-hour flight profile.

A three-hour ISR mission was generated to test the various controllers (see Fig 12). The flight profile includes a take-off, climb, cruise, endurance speed, high speed dash, descent, and landing. The ISR segment is split into two different segments to simulate the observation of two different ground locations. The cruise speed is designed to be 50 kts and the endurance speed 25 kts. At endurance speed, the hybrid-electric UAV operates in electric-only (stealth) mode. The design altitude is 5 kft mean sea level (MSL) and for this flight profile, the UAV takes off from 3.5 kft MSL.
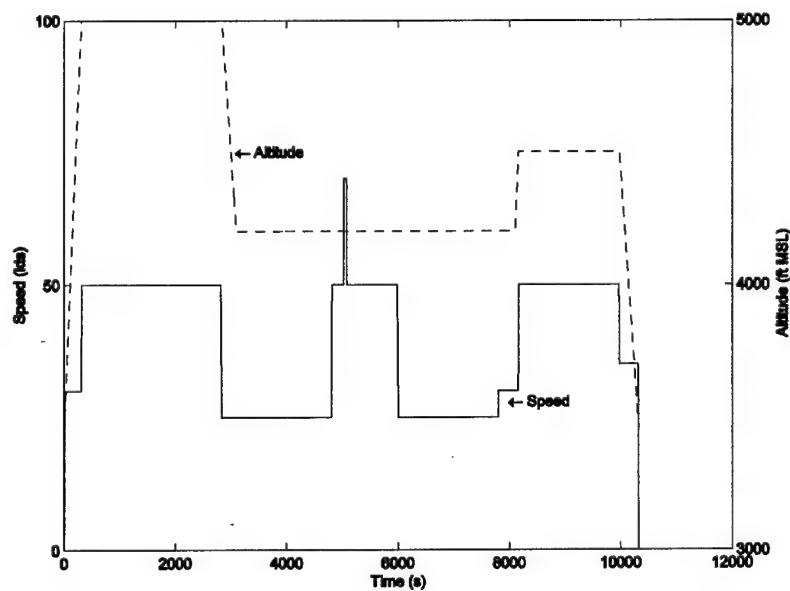
Fig. 12   Three-hour flight profile

B. Simulation Results for One-Hour ISR Mission

The hybrid-electric propulsion system controllers use a CD strategy for the one-hour ISR mission. The rule-based strategy does not use any additional CS logic for this mission. The CMAC controller uses the CD control surface. The rule-based controller is the baseline for the hybrid-electric propulsion system controllers and the CMAC controller improves on the rule-based controller. The CMAC controller surfaces are generated for sea-level operation. First-order approximations are used to adjust the torque output commands for the engine to the appropriate altitude.

The simulation results for the CMAC controllers reveal that they use less electrical energy than the rule-based controller. The engine operating points for the CMAC controller (L=19) are shown in Fig. 13. The torque has been adjusted to sea level. The commands near the IOL don't fall precisely on the IOL due to the CMAC control surface approximation.
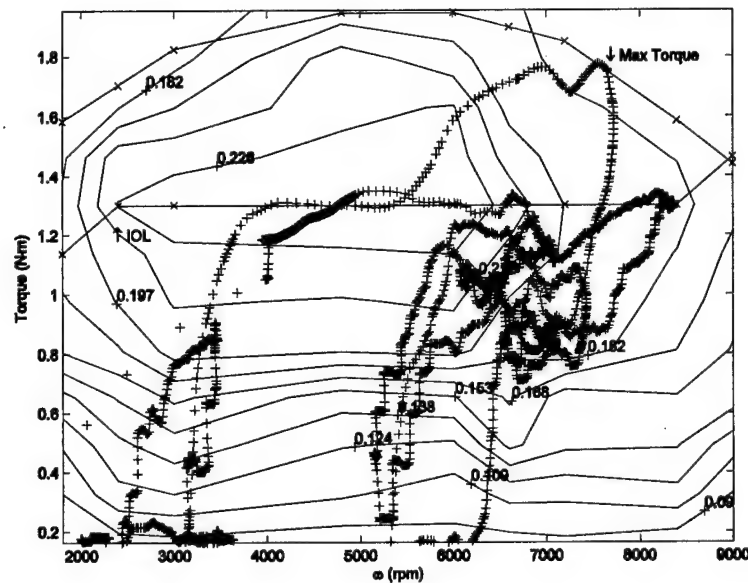
Fig. 13   Engine operating points, one-hour ISR mission, four-stroke, charge-depletion, CMAC controller (L=19)

A summary of the energy use for the one-hour ISR mission is listed in Table 7. Since the flight profile takes advantage of the CD logic or controller surfaces, much less energy is used for the hybrid-electric configurations than the original (ICE only) configuration. The HEUAV with the rule-based controller uses 54% less energy than the original configuration. The HEUAV with the CMAC controller (L=19) uses 58% less energy than the original configuration and 8.4% less than the HEUAV with the rule-based controller. The large decrease in energy use is due to the CD surfaces since no energy stored in the gasoline is used to maintain the battery charge.

Table 7   Energy summary for one-hour flight profile, four-stroke

Energy Type	Engine Only	Rule-Based	CMAC Controller, Charge-Depletion				
			L=3	L=7	L=9	L=14	L=19
Fuel (g)	192.3	70.4	60.5	60.7	61.0	61.7	60.3
Fuel (kWh)	2.29	0.844	0.725	0.728	0.732	0.740	0.723
Electricity (kWh)	N/A	0.202	0.238	0.238	0.238	0.236	0.239
Total (kWh)	2.29	1.05	0.963	0.965	0.969	0.976	0.962

C. Simulation Results for Three-Hour ISR Mission

The rule-based controller provides a baseline for the HEUAV results for the three-hour mission. CS is allowed through-out the mission to provide sufficient electrical energy during the two half-hour ISR mission segments. The amount of CS is dependent on the battery SOC since a proportional-derivative (PD) controller is used to control the amount of extra torque the engine produces for recharging. Due to the PD controller, the rate of charging increases as the SOC decreases. The logic keeps the SOC above 15%. The rule-based controller manages the storage of electrical energy sufficiently for the hybrid-electric system but the CMAC neural network controller improves on the rule-based controller.

Simulations using the CMAC controller were completed for L=3, 7, 9, 14, and 19. For L=19, the torque commands were not sufficient for the HEUAV to complete the mission. The battery SOC for the different controllers is shown in Fig. 14. During the cruise mission segment an error in the approximation will cause a difference in the amount of recharging. For L=19, the approximation causes insufficient recharging. However, for L=3, 7, 9 and 14, the battery SOC follows a similar path as for the optimization (i.e. LUT) results. All of the simulations end with a battery SOC near 20%. This permits a relatively accurate comparison to be made between the different controllers.

For the CMAC controller, the recharging is completed at a relatively constant rate as compared to the rule-based controller. Since the rule-based controller uses a PD algorithm, the rate increases as the SOC decreases. For the CMAC controllers, the rate is relatively constant throughout the SOC range. This keeps the engine running at a more continuous power level. Since the CMAC controllers keep the SOC near a constant SOC, most of the recharging is used to provide power to the avionics, flight control system, and the payload.
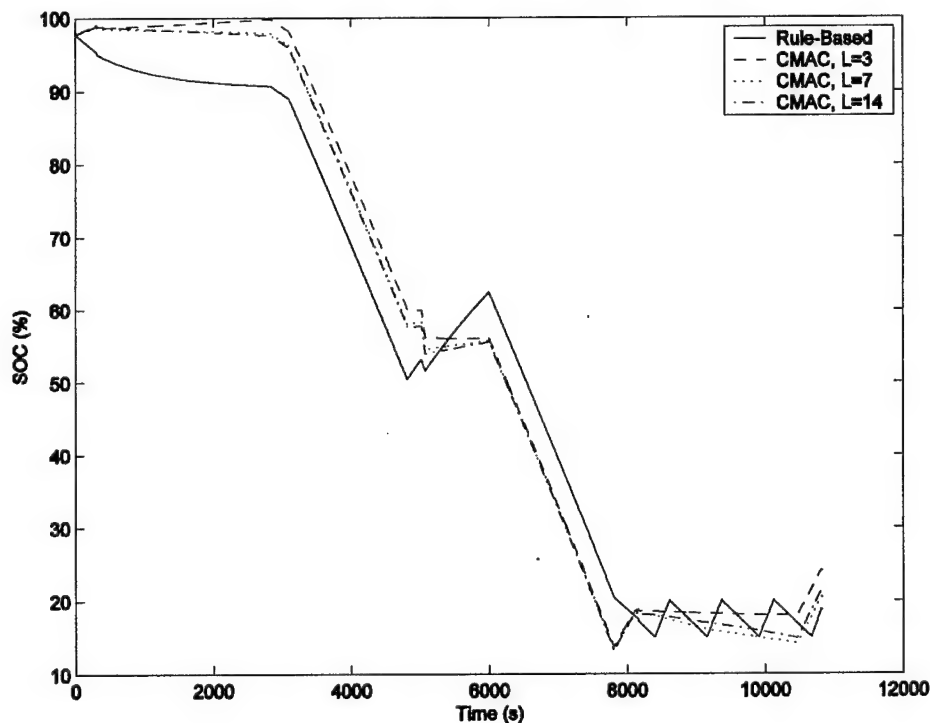
Fig. 14   Battery SOC, three-hour ISR mission, four-stroke engine, rule-based and CMAC controllers

The engine operating points for the CMAC controller (L=14) during the three-hour mission are shown in Fig. 15. The torque has been adjusted to sea level. As compared to Fig. 13, the CS control surface keeps the engine operating near the IOL much more often to recharge the battery pack.

The energy use for the three-hour ISR mission using the different controllers is shown in Table 8. The energy use shows that the original configuration uses the most energy. The energy use for the HEUAV using the rule-based controller is 22% less than the original configuration. The energy use for the HEUAV with the CMAC controller

(L=14) is 27% less than the original configuration and 5.8% less than the HEUAV with the rule-based controller. The CMAC approximations are close to the optimization results and show that a generalization factor up to 14 can be used. Values of L=7, 9, or 14 still provide reasonable results and use less energy as compared to the rule-based controller.
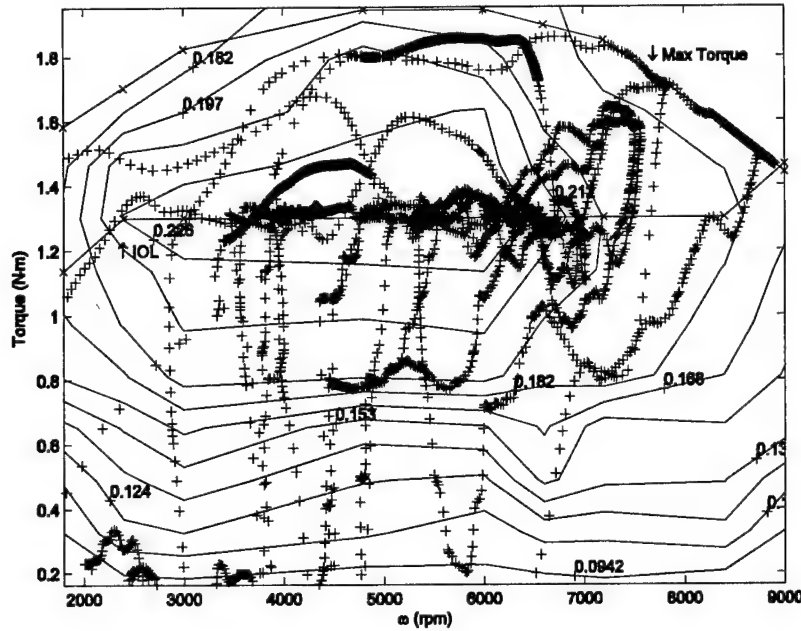

Fig. 15   Engine operating points, three-hour ISR mission, four-stroke, charge-sustaining, CMAC controller (L=14)

Table 8   Energy use summary for three-hour ISR mission, four-stroke engine

Energy Type	Engine Only	Rule-Based	CMAC Controller, Charge-Sustaining			
			L=3	L=7	L=9	L=14
Fuel (g)	779.3	582.1	548.4	545.9	541.9	547.1
Fuel (kWh)	9.27	6.98	6.57	6.54	6.50	6.56
Electricity (kWh)	N/A	0.240	0.244	0.245	0.265	0.246
Total (kWh)	9.27	7.22	6.82	6.79	6.76	6.80

VIII.   Conclusion

A conceptual design of a small UAV with a parallel hybrid-electric propulsion system, an optimization routine for the energy use of the propulsion system, the application of a CMAC neural network to approximate the optimization results, and simulation results were provided in this paper. Extensions to this research include dynamometer testing, variable-pitch propeller testing, and additional work on the CMAC neural network controller.

As UAVs are used for more applications, computerized dynamometer test stands will be needed to test more fuel efficient ICE and propulsion systems. The commercially available dynamometers are expensive since they need to be reliable and accurate with the capability to convert all data to standard day atmosphere to permit comparisons to simulation data. The development of an advance dynamometer test stand for UAV propulsion systems would provide an excellent research project and extension to this research.

A fixed-pitch propeller was used in the HEUAV model but as with most propellers, it operates at its peak efficiency over a short range of advance ratio. For the HEUAV, the advance ratio was similar at cruise and endurance speed. However, at other speeds that may be required for various missions, the propeller may not operate

near its maximum efficiency. A variable-pitch propeller permits a high efficiency over a wider range of advance ratio. The desired pitch could be an output from the hybrid-electric propulsion system controller.

The CMAC neural network controller developed in this research is trained off-line. The weights for the association memory of the CMAC controller can then be directly transferred to the memory of the embedded microcontroller. If the torque output of the ICE and EM is measured or estimated, then an adaptive controller could be developed to optimize the energy use in real-time. As the atmospheric conditions change, the torque output of the engine could be varied to optimize the energy use in real-time to increase the range of the UAV.

Depending on the resulting hyper-plane surface, a uniform input space for the CMAC controller may not be sufficient. Higher resolution may be needed for the surface in certain areas, especially where discontinuities exist. A nonlinear placement strategy can account for the discontinuities in the training data.

Acknowledgments

References

[1]Chan, C. C. and Chau, K. T., *Modern Electric Vehicle Technology*, Oxford, New York, Oxford University Press, 2001.

[2]Aldridge, E. C. and Stenbit, John P., "Unmanned Aerial Vehicles Roadmap: 2002-2027," Office of the Secretary of Defense, 2003.

[3]Perazzola, Carl, "Tomorrow's Ground Power Today," SAE June TOPTEC Conference, 2002.

[4]Wilson, J. R., "UAVs: A Worldwide Roundup," *Aerospace America*, 2003, pp. 30-35.

[5]Francisco, Avernethy Bellaflor, "M.S. Thesis: Implementation of an Ideal Operating Line Control Strategy for Hybrid Electric Vehicles," *Dept. of Aeronautical and Mechanical Engineering*, Davis, CA, University of California-Davis, 2002.

[6]Frank, Andrew A., "Control Method and Apparatus for Internal Combustion Engine Electric Hybrid Vehicles," *USPTO Patent Database*, USA, The Regents of the University of California, 2000.

[7]Frank, Andrew A., "Charge Depletion Control Method and Apparatus for Hybrid Powered Vehicles," *USPTO Patent Database*, USA, The Regents of the University of California, 1998.

[8]Husain, Iqbal, *Electric and Hybrid Vehicles Design Fundamentals*, Boca Rotan, Florida, CRC Press, 2003.

[9]Burke, A. F., "Hybrid/Electric Vehicle Design Options and Evaluations," *SAE Document SP-915*, 1992, pp. 53-77.

[10]Kim, Chunho, NamGoong, Eok, Lee, Seongchul, Kim, Talchol, and Kim, Hyunsoo, "Fuel Economy Optimization for Parallel Hybrid Vehicles with CVT," *SAE Paper 1999-01-1148*, 1999.

[11]Johnston, Brian, et al., "The Continued Design and Development of the University of California-Davis FutureCar," *SAE Paper 980487*, 1998.

[12]Kleback, Brian, Inman, Sara, and Noss, Ryan, "Design and Development of the 2002 Penn State University Parallel Hybrid Electric Explorer, the Wattmuncher," *SAE Paper 2003-01-1258*, 2003.

[13]Meyr, Nathaniel, et al., "Design and Development of the 2002 UC Davis FutureTruck," *SAE Paper 2003-01-1263*, 2003.

[14]Bond, Clayton, et al., "Design and Development of the 2003 University of Alberta Hybrid Electric Vehicle," *SAE Paper 2003-01-1268*, 2003.

[15]Matsuo, Isaya, Nakazawa, Shinsuke, Maeda, Hiromasa, and Inada, Eiji, "Development of a High-Performance Hybrid Propulsion System Incorporating a CVT," *SAE Paper 2000-01-0992*, 2000, pp. 1-9.

[16]Harmats, M. and Weihs, D., "Hybrid-Propulsion High-Altitude Long-Endurance Remotely Piloted Vehicle," *Journal of Aircraft*, vol. 36, 1999, pp. 321-331.

[17]Schurhoff, Robert Wayne, "M.S. Thesis: The Development and Evaluation of an Optimal Powertrain Control Strategy for a Hybrid Electric Vehicle," *Dept. of Aeronautical and Mechanical Engineering*, Davis, CA, University of California-Davis, 2002.

[18]Harmon, F.G., Frank, A.A., and Chattot, J.J., "Parallel Hybrid-Electric Propulsion System for an Unmanned Aerial Vehicle," AUVSI's Unmanned Systems North America 2004 Symposium, Anaheim, CA, 2004.

[19]Anderson, John D., *Aircraft Performance and Design*, Boston, MA, McGraw-Hill, 1999.

[20]Raymer, Daniel P., *Aircraft Design: A Conceptual Approach*, Washington, D.C, AIAA, 1992.

[21]Stinton, Darrol, *The Design of the Airplane*, 2nd ed, Reston, VA, AIAA, 2001.

[22]Corke, Thomas C., *Design of Aircraft*, Upper Saddle River, NJ, Prentice Hall, 2003.

[23]Gelhausen, P., "ACSYNT-A Standards-Based System for Parametric Computer Aided Conceptual Design of Aircraft," 1992 Aerospace Design Conference, Irvine, CA, 1992.

[24]Raymer, Daniel P. and Crossley, William A., "Variations of Genetic Algorithm and Evolutionary Methods for Optimal Aircraft Sizing," AIAA Aircraft Technology, Integration, & Operation Meeting, Los Angeles, CA, 2002.

[25]Ehsani, Mehrdad, Rahman, Khwaja M., and Toliyat, Hamid A., "Propulsion System Design of Electric and Hybrid Vehicles," *IEEE Transactions on Industrial Electronics*, vol. 44, 1997, pp. 19-27.

[26]Youngblood, J. W. and Talay, T. A., "Solar-Powered Airplane Design for Long-Endurance, High-Altitude Flight," AIAA 2nd International Very Large Vehicles Conference, Washington, D.C, 1982.

[27]Selig, Michael S., Donovan, John F., and Fraser, David B., *Airfoils at Low Speeds*, Virginia Beach, VA, H.A. Stokely, 1989.

[28]Eppler, Richard, *Airfoil Design and Data*, Berlin, Germany, Springer-Verlag, 1990.

[29]Siddiqi, S., Evangelista, R., and Kwa, T. S., "The Design of a Low Reynolds Number RPV," Low Reynolds Number Aerodynamics, Notre Dame, Indiana, 1989.

[30]Dev, S. Paul, "JP-8/Battery Hybrid Propulsion and Power for Small UAVs and UGVs," AUVSI's 30th Annual Unmanned Systems Symposium and Exhibition, Baltimore, MD, 2003.

[31]Harmon, Frederick G., "PhD Dissertation: Neural Network Control of a Parallel Hybrid-Electric Propulsion System for a Small Unmanned Aerial Vehicle," *Department of Mechanical and Aeronautical Engineering*, Davis, CA, University of California-Davis, 2005.

[32]Glanz, Filson H., Miller, Thomas W., and Kraft, L. Gordon, "An Overview of the CMAC Neural Network," IEEE Conference on Neural Networks for Ocean Engineering, 1991.

[33]Miller, Thomas W., Glanz, Filson H., and Kraft, L. Gordon, "CMAC: An Associative Neural Network Alternative to Backpropagation," *Proceedings of the IEEE*, vol. 78, 1990, pp. 1561-1567.

[34]Shiraishi, Hitoshi, Ipri, Susan L., and Cho, Dong-il D., "CMAC Neural Network Controller for Fuel-Injection Systems," *IEEE Transactions on Control Systems Technology*, vol. 3, 1995, pp. 32-38.

[35]Iwan, Laura C. and Stengel, Robert F., "The Application of Neural Networks to Fuel Processors for Fuel-Cell Vehicles," *IEEE Transactions on Vehicular Technology*, vol. 50, 2001, pp. 125-143.

[36]Miller, W. Thomas, "Real-Time Neural Network Control of a Biped Walking Robot," *IEEE Control Systems Magazine*, vol. 14, 1994, pp. 41-48.

[37]Kraft, L. Gordon and Dietz, Darryl, "Time Optimal Control Using CMAC Neural Networks," American Control Conference, Baltimore, MD, 1994.

[38]White, David A. and Sofge, Donald A., *Handbook of Intelligent Control: Neural, Fuzzy, and Adaptive Approaches*, New York, Van Nostrand Reinhold, 1992.

[39]Albus, J. S., "Data Storage in the Cerebellar Model Articulation Controller (CMAC)," *Journal of Dynamic Systems, Measurement, and Control*, vol. 63, 1975, pp. 228-233.

[40]Albus, J. S., "A New Approach to Manipulator Control: The Cerebellar Model Articulation Controller (CMAC)," *Journal of Dynamic Systems, Measurement, and Control*, vol. 63, 1975, pp. 220-227.

[41]Brown, Martin and Harris, Chris, *Neurofuzzy Adaptive Modelling and Control*, New York, Prentice Hall, 1994.

[42]Burgin, George, "Using Cerebellar Arithmetic Computers," *AI Expert*, vol. 7, 1992, pp. 32-41.

[43]Parks, P.C. and Militzer, J., "Improved Allocation of Weights for Associative Memory Storage in Learning Control Systems," *IFAC Design Methods of Control Systems*, 1991, pp. 507-512.

Web News   Images   Desktop   Encarta

CMAC Neural Network Structure

+Search Builder   Settings   Help   Español

Web Results
1-10 of 1,625 containing **CMAC Neural Network Structure** (0.30 seconds)

Fundamentals of Artificial Neural Networks
... Maps with Problem Dependent Cell **Structure**," in Artificial **Neural** Networks, Proc. of the 1991 Int. Con
Implementation of a High Speed **CMAC Neural Network** Using Programmable CMOS Logic Cell ...
neuron.eng.wayne.edu/tarek/MITbook/ref/refs.html   Cached page

Robotics /Vib Cntrl HOME
... ten degree of freedom biped walking **structure**, with force sensing feet and a two-axis ... grant for $365
apply a **neural network** called **CMAC** to the area of vibration control. The NSF ...
www.ece.unh.edu/robots/rbt_home.htm   Cached page

IEEE International Conference on Fuzzy Systems 2001
... PCMNN: A Parallel Cooperative Modularied **Neural Network** Architecture. 268-271 BibTeX Yo-Ping Hu
Hung-Reng Lai , Ching-Chang Wong : A Fuzzy **CMAC Structure** and Learning Method for Function ...
www.sigmod.org/sigmod/dblp/db/conf/fuzzIEEE/fuzzIEEE2001.html   Cached page   1/23/2005

Soft Comput.
... 147   Interrogating the **structure** of fuzzy cognitive maps by ... 565   Fuzzy system and **CMAC netwo**
spline membership ... Application of generalised **neural network** for aircraft landing ...
wotan.liu.edu/docis/dbl/softco/index.html   Cached page   1/23/2005

http://www.garfield.library.upenn.edu/histcomp/self_org_maps/index-aus.html
... Osowski S Gas analysis system composed of a solid-state sensor array and hybrid **neural network str**
3010 1997 BIOLOGICAL CYBERNETICS 77(6):433-446 Bruske J; Hansen M; Riehn L; Sommer G ...
www.garfield.library.upenn.edu/histcomp/self_org_maps/index-aus.html   Cached page   1/24/2005

http://www.garfield.library.upenn.edu/histcomp/self_org_maps/index-lcs.html
... 454-466 NOVIC M; ZUPAN J INVESTIGATION OF INFRARED SPECTRA-**STRUCTURE** CORREI
USING KOHONEN AND COUNTERPROPAGATION **NEURAL-NETWORK** 33 13 3 2338 1995 NEUI
NETWORKS 8(5):729-743 BEZDEK JC; PAL NR 2 SOFT ...
www.garfield.library.upenn.edu/histcomp/self_org_maps/index-lcs.html   Cached page
Show more results from "www.garfield.library.upenn.edu".

Program IASTED Applied Informatics Conference
... 247 Rainfall Forecast using a **Neural Network** with a Real-coded Genetical Preprocessing S ... term W
Forecasting using **CMAC Structure** N. Sarmadi and N. Teshnehlab (Iran) 351-327 ...
www.iasted.org/conferences/2002/austria/program-351f.htm   Cached page   1/24/2005

Faculty Publications
... and Compensation on Machine Tools by **CMAC Neural Network**," Int. J. Machine Tools and Manufactu
Monte Carlo Simulation of Weldment Micro-**structure**," Proc. Third Africa-USA Int. Conf. on Mfg ...
me.engin.umich.edu/news/pubs/ar/1996-1997/manuf.html   Cached page   1/25/2005

Bibliography
... Agre, 1988 Agre, P. E. (1988). The Dynamic **Structure** of Everyday Life . PhD thesis ... P. (1990). A su

hybrid-electric propulsion system for small UAV

Web Results
1-9 of 330 containing **hybrid-electric propulsion system for small UAV** (0.15 seconds)

AUVSI - News
... up to 20 MPH.   The **small UAV** includes an autopilot ... ducted-rocket ramjet **propulsion system** into ɑ sector including **propulsion** systems for electric, **hybrid electric** and fuel cell electric ...
www.auvsi.org/news/index.cfm Cached page 1/22/2005

03.1 SITIS Archive Page
... Modeling of **Propulsion System** and Drive Train Clutch Systems for ... and Metering for Very **Small U/** N03-092 ... Combatants & N03-119 **Hybrid Electric** Drive for **Small** Craft # N03-120 New Low ...
www.dtic.mil/matris/sbir/sbir031/sbirqs031.html Cached page

DARPA 2002
... Fuel, Compression Ignition **Small UAV** Engines Advanced **Propulsion** Technologies, Inc. P. O. Box 3C Weight, JP-8 Fueled **Hybrid Electric Propulsion System** for UAVs G & G Technology, Inc. 1169 ...
www.arpa.mil/sbir/02.2Awards.htm Cached page

Army FY 03.2 SBIR Solicitation
... Health and Usage Monitoring **System** (HUMS) for Unmanned Aerial Vehicles (**UAV**) A03-075 ... Energɣ The **system** should be as **small** (volumetrically) as possible and ...
www.acq.osd.mil/sadbu/sbir/solicitations/sbir032/army032.htm Cached page

AF - 470 Phase I Selections from the 04.1 Solicitation
... **UAV**). Such antennas need to reach as low as VHF ... Title: Turbo-Hybrid-Rocket **Propulsion** for **Smal** Vehicle Operations ... be definition of a THR **propulsion system** capable ...
www.dodsbir.net/selections/abs041/afabs041.htm Cached page

Northrop Grumman Demonstrates Key Technologies For Army Unmanned Armed
... Rucker, Aviation and Missile R&D **UAV system** program managers and P Executive ... the U.S. Marine develop a **hybrid electric propulsion system** to power **small** unmanned ground combat vehicles ...
www.spacedaily.com/news/unmanned-combat-04e.html Cached page 1/23/2005

DIAR.com - News Archive 2002
... 20.12.02] 'PREDATOR B' **UAV** SURVEILLANCE/ATTACK **SYSTEM** INTO CONTRACT: General ... AR ERECTION/**PROPULSION** BOATS: ADI Limited has been ... subsystems and produces **hybrid electric** d for ...
www.diar.com/data/news02.htm Cached page

Index
... 2004 Featured Articles **Small** Particle May Answer Large ... aerial vehicle (**UAV**), Wide-Area Tracking ς (WATS). Research Highlights It's ... vehicles, electrolysis, **hybrid-electric** car, hydrogen fuel. ...
www.llnl.gov/str/Indexlist.html Cached page 1/23/2005

Aeronautics Technology
... would allow routine **UAV** flight operations in ... capabilities for a **small** aircraft transportation **system**. 5/ Complete ... systems, and **hybrid electric propulsion** systems. (P&P) $M 84.60 147 ...
www.nasa.gov/pdf/55403main_20%20AT.pdf Cached page PDF file 1/23/2005

Web News   Images   Desktop   Encarta

hybrid-electric vehicle

+Search Builder   Settings   Help   Español

Web Results

1-10 of 59,160 containing **hybrid-electric vehicle** (0.31 seconds)

SPO

NREL: Advanced Vehicles and Fuels Research - Hybrid Electric and Fuel ...

... research supports the U.S. Department of Energy's FreedomCAR & **Vehicle** Technologies Program . NREL works toward developing **hybrid electric** vehicles (HEVs) and fuel cell vehicles (FCVs); moving them from ...
www.nrel.gov/vehiclesandfuels/hev Cached page

Green Hybrid: Gas-Electric Cars › Central

The comprehensive resource for **hybrid electric vehicle** information. Explore our content or interact with others while discussing the gasoline-electric technology. About the Creator Advertise | Contact ...
greenhybrid.com Cached page

EV World: The World of Electric, Hybrid, Fuel Cell and Alternative ...

... Some Commuters, Electric Cars Worth the Switch UQM Technologies Drive New **Hybrid Electric** Transit Buses 21st Electric **Vehicle** Symposium in Monaco Will Crossovers and Hybrids Live Up To Their Hype? Accord ...
www.evworld.com 1/24/2005

FreedomCar: Advanced Vehicle Testing Activity

... Expert The primary goal of the Advanced **Vehicle** Testing Activity (AVTA) is to benchmark and ... compressed natural gas-blended fuels **Hybrid electric**, pure electric, and hydraulic drive systems ...
ev.inel.gov Cached page 1/24/2005

Hybrid Electric Vehicle (HEV)

... the third year of Tech's participation, Texas Tech was selected to participate in the **Hybrid Electric Vehicle** (HEV) competition. For the 1993 and 1994 contests, students researchers modified a Ford ...
www.osci.ttu.edu/ME_Dept/hev.htmld Cached page 1/23/2005

Hybrid-Electric Vehicle Demand To Reach 4.5 Million Units in 2013

... primary stimulants: rising energy costs and increased emissions regulations. ENERGY TECH **Hybrid-Electric Vehicle** Demand To Reach 4.5 Million Units in 2013 Energy costs and increased emissions regulations ...
www.spacedaily.com/news/energy-tech-05a.html Cached page 1/24/2005